Coupled deformation-diffusion effects in the mechanics of faulting and failure of geomaterials

JW Rudnicki

Department of Civil Engineering, Northwestern University, 2145 Sheridan Rd, Evanston IL 60208-3109; jwrudn@northwestern.edu

This review article discusses the applications of poroelasticity to the mechanics of faulting and failure in geomaterials. Values of material parameters inferred from laboratory and field studies are summarized. Attention is focused on solutions for shear dislocations and shear cracks. A common feature is that undrained response, invoked by rapid slip or deformation, is stiffer than drained response, which occurs for slower slip or deformation. The time and spatial variation of the stress and pore pressure is different for slip on permeable and impermeable planes. These solutions are applied to interpretation of water well level changes due to slip, earthquake precursory processes, and stabilization of spreading slip zones. Inclusion models for reservoirs, aquifers, and other inhomogeneities are formulated and the results are applied to stress and strain changes caused by fluid mass injection or withdrawal. This article has 120 references. [DOI: 10.1115/1.1410935]

1 INTRODUCTION

The shallow parts of the earth's crust are mostly infiltrated by fluids and the coupling of fluid flow with deformation of the crust alters the response. In particular, this coupling introduces a dependence on time into the response, in addition to any time-dependence of the solid matrix itself. Deep drill holes have encountered significant quantities of fluid at surprisingly large depths, nearly 10 km [1,2], and geochemical analysis of fluids associated with the faults in California [3] suggest that the fluids originated from the mantle. Consequently, this coupling may be a significant effect not only at shallow depths but throughout the crust.

Coupling of fluid flow with deformation has been associated with a large variety of geomechanical and geophysical problems [4]. Roeloffs [5] has reviewed observations of hydrologic precursors to earthquakes, Roeloffs [6] has summarized poroelastic methods in the study of earthquake related phenomena, and a special section of the *Journal of Geophysical Research* [7] has been devoted to the mechanical involvement of fluids in faulting. Phenomena in which coupling between deformation and diffusion has played a significant role include response of water wells to earth tides and fault slip, earthquake initiation, precursors, and aftershocks, geyser periodicity [8], fault creep (aseismic slip), seismicity induced by reservoir loading and fluid injection or extraction, earthquake swarms [9], and triggering of earthquakes and landslides by dike intrusion [10,11]. Recently, there have been suggestions that the build-up and release of pore pressure may mediate the occurrence of some earthquakes [12,13] and Zhao *et al* [14] have used seismic techniques to infer the presence of pressurized fluids at the hypocenter of the Kobe earthquake. Synthetic aperture radar (SAR) has made possible full field observations of crustal deformation on a time scale of fluid diffusion. For example, Peltzer *et al* [15] attribute observations of postseismic rebound by SAR near the Landers, California, earthquake to pore fluid flow. In addition, changes in magnetic field, resistivity, and chemistry near faults [16] may be associated with fluid flow.

The coupling of deformation of diffusion with deformation is also a significant aspect of technological problems involving the injection or extraction of fluids from the crust. Typical examples are hydraulic fracturing and the response of pressurized boreholes but also a variety of other problems associated with the production and storage of hydrocarbons, disposal of waste products, both radioactive and chemical, in wells, and managment of aquifer pumping for irrigation. A novel application, prompted by concerns about the adverse effects of anthropogenic carbon dioxide emissions on climate, is the sequestration of CO_2 in depleted or inactive oil and gas reservoirs or deep saline aquifers. Although injection of CO_2 is often used to enhance hydrocarbon production, the efficient and safe injection of large volumes for sequestration of periods on the order of 100 years requires a better understanding [17] of not only mechanical, but also chemical interaction of flow on porosity, permeability, and existing fractures and faults.

The assumptions of linear poroelasticity, namely linear elastic behavior of the matrix and constant, though possibly

Transmitted by Associate Editor PM Adler

non-uniform, permeability, may be appropriate only within a limited range of conditions. Often, inelastic volume changes occur, possibly associated with inelastic shear deformation, and changes in mean stress can cause significant alterations in permeability, especially if the fluid flow is primarily through long, thin fractures. In spite of these limitations, linear poroelasticity is a valuable framework for assessing the effects of coupling between deformation and diffusion, interpreting field and laboratory data, and making predictions of *in situ* behavior. Certainly, when coupling is thought to be important, linear poroelasticity is a significant improvement over formulations that neglect coupling altogether and either treat deformation as independent of flow or consider flow through a non-deforming matrix. Furthermore, the difficulties of getting reliable properties *in situ* and their spatial variation often make consideration of more elaborate models unwarranted.

This paper reviews the effects of coupling between deformation and pore fluid diffusion on geomechanical processes from the point of view of some relatively simple solutions. Attention is focused primarily on linear poroelasticity, but some inelastic effects are also discussed.

2 FORMULATION

2.1 Constitutive relations

The equations of linear poroelasticity were first formulated in generality by [18]. A recent thorough discussion of them has been given by [19]. Coussy [20] develops the linear theory within a more general framework of the mechanics of porous continua and Wang [21] discusses in detail the relation of Biot theory to a traditional hydrological approach. Although essentially the same in substance as Biot's treatment, the formulation of [22] emphasized the structure of the equations revealed by considering two limits: drained response (no alteration in pore fluid pressure), which is attained for deformations that are slow relative to the time scale of fluid mass diffusion, and undrained response (no alteration in fluid mass content), which is attained for deformations that are rapid (though quasi-static) relative to the time scale of fluid mass diffusion.

The equations of poroelasticity can also be developed from the point-of-view of mixture theory [23] but this approach requires knowledge or assumption about the microscale behavior of the constituents and appears to have little advantage when the solid constituent has a definite structure. In this case, the boundary of an element of porous material coincides with points of the solid skeleton and the displacement of these points defines the average strain of the element. Hence, it is natural to consider strains of the solid skeleton rather than strains of the individual solid and fluid constituents. Similarly, there is no need to decompose stresses into separate solid and fluid stresses. Rather, the equations can be formulated in terms of the total stress, derived from the force per unit area of porous material, and the pore pressure. As emphasized by [20], strains of the solid skeleton, total stresses and pore pressure are amenable to macroscopic determination whereas constitutent strains and stresses are not.

An element of porous solid, defined by points of the solid skeleton is depicted schematically in Fig. 1. The element is assumed to be large enough to be representative of the material but small enough so that the deformation is adequately approximated as homogeneous. Average strains of the solid skeleton ε_{ij} are defined by displacements of points of the boundary. Average total stresses σ_{ij} are defined so that the force per unit area of the boundary of the porous solid is $n_i\sigma_{ij}$ where the n_i are the components of the local unit normal. The element is imagined to be connected to a reservoir of homogeneous pore fluid with density ρ_f. The pore pressure p is defined as that pressure that must be applied to the reservoir to prevent any fluid mass exchange between the reservoir and element of porous solid. If the volume of the porous element is V_0 in the reference state, the mass of fluid contained in the porous element is mV_0.

For isothermal deformation, the change in Helmholtz potential of the entire system, comprising both the element of porous solid and the reservoir, is equal to the reversible work of the total stresses on the strains of the solid skeleton and that associated with any exchange of fluid mass between the reservoir and the porous element. This change is given by

$$d\psi = \sigma_{ij}d\varepsilon_{ij} + \mu dm, \tag{1}$$

where ψ is the Helmholtz energy per unit reference volume of porous solid and μ, the chemical potential or Gibb's function per unit mass of the fluid phase, is given by [24,25]

$$\mu = \int_{p_0}^{p} \frac{dp'}{\rho_f(p')} \tag{2}$$

The indicies (i,j) range over (1,2,3) and a repeated index denotes summation. The Helmholtz energy in (1) is a function of strains and fluid mass content. The stress and pore pressure can be used as independent variables by performing a Legendre transformation and introducing the potential $\psi' = \psi - \sigma_{ij}\varepsilon_{ij} - \mu m$. Changes in ψ' are given by

$$d\psi' = -\varepsilon_{ij}d\sigma_{ij} - v\,dp \tag{3}$$

where, following the nomenclature of [22], the apparent fluid volume fraction is $v = m/\rho_f$. The initial (reference) void vol-

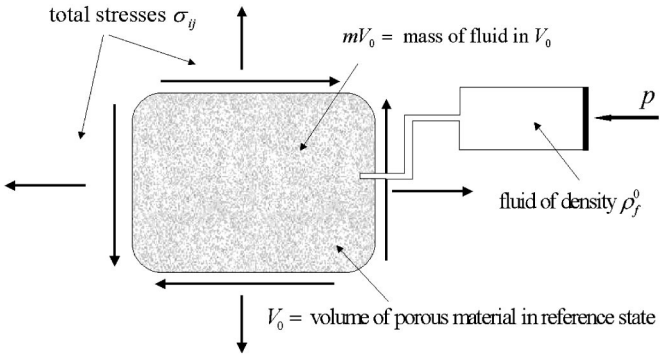

Fig. 1 Schematic illustration of an element of porous material connected to an imagined reservoir of homogeneous pore fluid

ume fraction v_0 is equal to the initial porosity accessible to fluid, ϕ_0. But because v is defined as the apparent void volume fraction *per unit reference volume*, $v-v_0$ is not identical to the first order change in porosity $\phi-\phi_0$. (My own appreciation of this owes much to unpublished notes of Dave McTigue from 1985.) Thus, $v=J\phi$, where J is the Jacobian of the deformation from the reference to current state and equal to the ratio of the current volume to reference volume. The linearized change in porosity is related to $v-v_0$ by

$$v-v_0=\phi-\phi_0+\phi_0\varepsilon_{kk}, \tag{4}$$

where $J\approx 1+\varepsilon_{kk}$ and ε_{kk} is the linearized volume strain.

The form (3) suggests that constitutive relations for ε_{ij} and v be written in terms of σ_{ij}, p. Furthermore, since ψ' is a potential, the requirement that the mixed second partial derivative with respect to σ_{ij} and p can be taken in either order yields the Maxwell relation

$$\frac{\partial\varepsilon_{ij}}{\partial p}=\frac{\partial v}{\partial\sigma_{ij}}. \tag{5}$$

In the limit of drained deformation, fluid mass exchange equilibrates any alteration in pore pressure. Consequently, the strain of the solid matrix ε_{ij} is given in terms of the total stress σ_{ij} by the usual relation of linear (isotropic) elasticity

$$\varepsilon_{ij}=\frac{1}{2G}\sigma_{ij}-\left(\frac{1}{2G}-\frac{1}{3K}\right)\frac{\sigma_{kk}}{3}\delta_{ij}, \tag{6}$$

where G is the shear modulus and K is the drained bulk modulus of porous material. The Kronecker delta, δ_{ij}, is equal to unity if $i=j$ and to zero, otherwise. In general, the pore pressure is not constant and a term linear in p must be appended to Eq. (6):

$$\varepsilon_{ij}=\frac{1}{2G}\sigma_{ij}-\left(\frac{1}{2G}-\frac{1}{3K}\right)\frac{\sigma_{kk}}{3}\delta_{ij}+\left(\frac{1}{3K}-\frac{1}{3K_s'}\right)p\,\delta_{ij}. \tag{7}$$

The notation is that of [22], who write $(1/K-1/K_s')$ for $1/H$ used by [18]. Alternatively, Eq. (7) can be rearranged as follows:

$$\sigma_{ij}=2G\varepsilon_{ij}+(K-2G/3)\,\delta_{ij}\varepsilon_{kk}-\zeta p\,\delta_{ij}, \tag{8}$$

where ζ, often denoted by the symbol α (*eg*, [19]), is $1-K/K_s'$. Recognizing that replacing σ_{ij} in Eq. (6) by $\sigma_{ij}+\zeta p\,\delta_{ij}$ yields Eq. (7) identifies this combination as the form of the *effective stress* appropriate for elastic strain [22,26].

Similarly, the alteration of the apparent volume fraction v from a reference value v_0 depends linearly and isotropically on the stress and the pore fluid pressure. The condition (5) requires that the coefficient of σ_{ij} in this relation be the same as the coefficient of p in Eq. (7). The coefficient of p is expressed in terms of an additional modulus K_s'':

$$v-v_0=\frac{\zeta}{K}\left(\frac{\sigma_{kk}}{3}+p\right)-\frac{v_0}{K_s''}p \tag{9}$$

where, again as noted by [22], v_0/K_s'' is related to Biot's R and H by $v_0/K_s''=1/H-1/R$.

The particular arrangement of the coefficients in Eqs. (7) and (9) and the meaning of the two moduli K_s' and K_s'' can be clarified by examining the strain due to the special loading $\sigma_{ij}=-\sigma\delta_{ij}$ and $p=\sigma$ [26,27]. For this loading, Eqs. (7) and (9) give

$$\varepsilon_{kk}=-\sigma/K_s' \tag{10a}$$

$$v-v_0=-v_0\sigma/K_s'' \tag{10b}$$

Rice and Cleary [22] note that if the void space is continuous and accessible to fluid, the solid phase is homogeneous and isotropic with bulk modulus K_s, and both the solid and fluid phases are chemically inert, this loading produces local isotropic compression of the solid phase. Thus, K_s' and K_s'' can be identified with K_s. More generally, however, K_s' and K_s'' must be regarded as phenomenological coefficients that could be determined via the procedures described by [28] for determining R and H.

The linearized change in fluid mass content per unit reference volume, $m=\rho_f v$, is

$$m-m_0=\rho_f^0(v-v_0)+v_0(\rho_f-\rho_f^0) \tag{11}$$

The linearized change in density of the pore fluid, from a reference value ρ_f^0, is

$$\rho_f-\rho_f^0=\rho_f^0 p/K_f \tag{12}$$

where K_f is the bulk modulus of the pore fluid. Substituting (9) and (12) into (11) yields

$$m-m_0=\rho_0 v_0\left(\frac{1}{K_f}-\frac{1}{K_s''}\right)p+\frac{\zeta\rho_0}{K}\left(\frac{\sigma_{kk}}{3}+p\right) \tag{13}$$

where, in this equation and henceforth, ρ_0 has been written for ρ_f^0. For undrained deformation, $m=m_0$ and the relation between the pressure and the mean normal stress is obtained from Eq. (13):

$$p=-B\sigma_{kk}/3 \tag{14}$$

The constant B, Skempton's coefficient, is given in terms of the various bulk moduli as

$$B=\frac{\zeta}{\zeta+v_0K(1/K_f-1/K_s'')} \tag{15}$$

After substituting (14) into (7), this equation can be rearranged in the form of (6) with K_u, the bulk modulus for undrained deformation, replacing K:

$$K_u=K/(1-\zeta B) \tag{16}$$

The shear modulus G is the same for both drained and undrained deformation (since pure shear tends to induce no net fluid mass flux from an element). The change in fluid mass content (13) can be rewritten in the following more compact forms using K_u:

$$m-m_0=\zeta\rho_0[\,\epsilon_{kk}+\zeta p/(K_u-K)] \tag{17}$$

$$m-m_0=\frac{\zeta\rho_0}{K}\left[\frac{\sigma_{kk}}{3}+\frac{K_u}{K_u-K}\zeta p\right] \tag{18}$$

Expressions for the drained and undrained Poisson's ratios can be obtained from the corresponding bulk moduli by means of the usual elasticity relation

$$\nu = \frac{3K - 2G}{2(3K + G)} \tag{19}$$

Using Eq. (19) with K_u yields an expression for ν_u, the Poisson's ratio for undrained response:

$$\nu_u = \frac{\nu + B\zeta(1-2\nu)/3}{1 - B\zeta(1-2\nu)/3} \tag{20}$$

Skempton's coefficient B satisfies $0 \leqslant B \leqslant 1$ and the undrained Poisson's ratio ν_u satisfies $\nu \leqslant \nu_u \leqslant 1/2$. In both cases, the upper limit is attained for separately incompressible solid and fluid constituents (typically, a good approximation for soils) and the lower for a very compressible pore fluid.

The constitutive formulation is completed by Darcy's law. In the absence of fluid mass body forces, Darcy's law states that the fluid mass flow in the ith direction per unit area of porous solid, q_i, is proportional to the gradient in pore pressure:

$$q_i = -\rho_0 \kappa \partial p / \partial x_i \tag{21}$$

Because the coefficient κ depends on both the fluid viscosity and the geometry of the fluid pathways, it is often expressed as k/χ, where χ is the fluid viscosity and k is a permeability with dimensions of length squared. Values of k are often given in darcies (1 darcy $= 10^{-8}$ cm^2). Alternatively, κ can be expressed as $\bar{k}/\rho_0 g$ where g is the acceleration of gravity and $\bar{k}$ has the dimensions of velocity. This form is particularly convenient for gravity flows in which case $\bar{k}$ has the interpretation of the volume flow rate per unit area due to a pressure gradient $\rho_0 g$.

2.2 Field equations

The relevant field equations are the usual ones of solid mechanics, equilibrium, and strain displacement, and, in addition, conservation of fluid mass. Equilibrium is expressed as

$$\sigma_{ij,i} + F_j(\mathbf{x},t) = 0, \tag{22}$$

where F_j is the body force per unit volume and $(\ldots)_{,i}$ denotes $\partial(\ldots)/\partial x_i$. The infinitesimal strain is related to the displacement gradient by

$$\epsilon_{ij} = (u_{i,j} + u_{j,i})/2. \tag{23}$$

Conservation of fluid mass is

$$q_{k,k} + \partial m / \partial t = Q(\mathbf{x},t) \tag{24}$$

where Q is a fluid mass source.

Substitution of (23) into (8) and the result into (22) yields

$$(K + G/3)e_{,j} + Gu_{j,ii} + F_j - \zeta p_{,j} = 0 \tag{25}$$

where $e = \varepsilon_{kk} = u_{i,i}$ is the dilatation. As recognized by Geertsma [29], gradients in pore pressure act as a distribution of body forces. Consequently, if the distribution of pore pressure is known, the displacements and stresses can be determined by superposition of the solution of (25) for a Dirac singular distribution of body force (point force). Because it is the *gradient* of the pore pressure that acts as a body force, the result can be reduced to the superposition of a distribution of centers of dilatation [29]. Geertsma [29,30] determined the surface displacement due to a uniform reduction of pressure in a tabular (flat, axisymmetric) zone and used the results to analyze observed subsidence over compacting reservoirs. Segall [31,32] has used the same approach to determine the stress changes outside a reservoir caused by pressure reductions. Segall *et al* [33] show that the predicted stress changes are consistent with observed seismicity near the Lacq gas field in southwestern France.

Substituting Darcy's law (21) into (24) gives

$$-\rho_0 \kappa p_{,kk} + \partial m / \partial t = Q(\mathbf{x},t) \tag{26}$$

where it has been assumed that the permeability is uniform. Equation (17) and the divergence of Eq. (25) can be used to eliminate p from Eq. (26). The result is

$$c m_{,kk} - \partial m / \partial t = Q(\mathbf{x},t) - \frac{\rho_0 \kappa (K_u - K)}{\zeta (K_u + 4G/3)} F_{k,k} \tag{27}$$

where the diffusivity c is

$$c = \kappa \frac{(K_u - K)(K + 4G/3)}{\zeta^2 (K_u + 4G/3)} \tag{28}$$

[34]. Rice and Cleary [22] give another useful expression for c in terms of G and the Poisson's ratios ν and ν_u:

$$c = \kappa \left[\frac{2G(1-\nu)}{(1-2\nu)}\right]\left[\frac{B^2(1+\nu_u)^2(1-2\nu)}{9(1-\nu_u)(\nu_u - \nu)}\right]. \tag{29}$$

They remark that the second bracket is unity for incompressible constituents ($B = 1$, $\nu_u = 1/2$) and the first bracket is the elastic modulus for uniaxial strain. Other equivalent expressions for the diffusivity have been given by [35,36]. As observed by [37], the divergence of body force field in Eq. (27), equivalent to a distribution of centers of dilatation, contributes a source term to the equation for diffusion of fluid mass. Alternatively, Eq. (17) can be used to eliminate p from (25) in favor of m:

$$(K_u + G/3)e_{,j} + Gu_{j,ii} + F_j - \frac{(K_u - K)}{\zeta \rho_0} m_{,j} = 0. \tag{30}$$

Segall [38] has used the solution of the one-dimensional version of Eq. (27) without body forces and with a source term to model fluid extraction at a constant rate from a thin producing layer. He substitutes the solution for m into (30) (again without body forces) and uses a Green's function approach to solve for the stress and pore pressure changes and surface displacements in a plane strain half-space due to fluid mass extraction. The results are used to analyze the effects of fluid mass extraction in the epicentral region of the 1983 Coalinga earthquake. Although Segall [38] concludes that the calculated stress and pore pressure changes do not support the hypothesis that the Coalinga earthquake was induced by fluid extraction, he does suggest [31] that, in general, fluid extraction can trigger earthquakes even though the pore pressure in the reservoir is decreasing.

2.3 Plane strain

Two-dimensional solutions can provide a reasonable idealization of a variety of geomechanical problems. An important simplifying feature of the plane strain formulation, noted by [22], is that the governing equations can be expressed entirely in terms of the stress and pore pressure. For plane strain deformation in the xy plane, the compatibility equation, in the absence of body forces, can be expressed as

$$\nabla^2(\sigma_{xx}+\sigma_{yy}+2\eta p)=0 \tag{31}$$

and the fluid mass diffusion equation, without source terms, becomes

$$(c\nabla^2-\partial/\partial t)[\sigma_{xx}+\sigma_{yy}+(2\eta/\mu)p]=0 \tag{32}$$

where $\nabla^2(\ldots)$ is the two-dimensional Laplace operator and the material constants enter only in the combinations

$$\eta=3(\nu_u-\nu)/2B(1+\nu_u)(1-\nu) \tag{33}$$

$$\mu=(\nu_u-\nu)/(1-\nu) \tag{34}$$

If the boundary conditions can be expressed in terms of the stress and pore pressure, then (31) and (32) and two of the three equilibrium equations (22) suffice to determine the pore pressure and the three in-plane stress components.

3 VALUES OF MATERIAL PARAMETERS

The constitutive relations for an isotropic, linear poroelastic material introduce two parameters in addition to the usual ones of linear elasticity. These may be taken as ν_u and B, or ζ and K_u. In the special cases that the bulk moduli K_s' and K_s'' can be identified with the bulk modulus of the solid constituents K_s, then these additional constants can be calculated from measurements of the drained shear and bulk moduli, G and K, the porosity v_0, and the bulk moduli of the solid and fluid constituents K_s and K_f. In general, however, the additional parameters must be measured. Detournay and Cheng [19] and Wang [21] discuss the standard tests for obtaining them.

Table 1 tabulates values of ν, ν_u, and B for the rocks listed by [22] and values for a Boise sandstone inferred by [39] from data of [40–42]. Also listed is the ratio $(1-\nu)/(1-\nu_u)$, which appears prominently in many plane strain solutions. Its excess over unity is a measure of the magnitude of difference between drained and undrained response. The final column lists the values of the second quantity in square brackets in (29). Recall that this is unity for incompressible constituents. The last two rows list values adopted by [43] as representative of rock and gouge.

Roeloffs [44] discusses measurements of B for several rock types by [45,46]. Both find that B decreases with increasing effective compressive stress, by as much as 40 to 60% at 10 MPa effective compressive stress. Mesri *et al* [45] also found that estimates of B from (15), with $K_s'=K_s''=K_s$, decreased with effective compressive stress but were larger than measured values. In contrast, Green and Wang [46] find that the estimates agreed well with their measurements. To estimate the effects of increasing effective stress on ν_u and B, Roeloffs [5] calculates these values using Eqs. (20) and (15), with $K_s'=K_s''=K_s$, and compressibility measurements of [47] on Westerly granite and Stone Mountain granite. For the Westerly granite, she finds that B decreases from 0.55 to 0.23 as the effective stress increases from 100 MPa to 200 MPa while ν_u remains essentially unchanged. For the Stone Mountain granite, B decreases from 0.99 to 0.38 and ν_u decreases from 0.458 to 0.252 as the effective stress increases from zero to 200 MPa.

Table 1. Values of material parameters

Rock Type	ν	ν_u	B	$\frac{(1-\nu)}{(1-\nu_u)}$	$\frac{B^2(1+\nu_u)^2(1-2\nu)}{9(1-\nu_u)(\nu_u-\nu)}$
Tennessee Marble	0.25	0.27	0.51	1.03	1.60
Westerly Granite	0.25	0.34	0.85	1.14	1.21
Charcoal Granite	0.27	0.30	0.55	1.04	1.24
Ruhr Sandstone	0.12	0.31	0.88	1.28	0.86
Berea Sandstone	0.20	0.33	0.62	1.19	0.52
Weber Sandstone	0.15	0.29	0.73	1.20	0.69
Boise Sandstone	0.20	0.34	0.51	1.25	0.34
rock	0.2	0.3	0.8	1.14	1.03
gouge	0.2	0.4	0.9	1.33	0.88

A difficulty in applying these values to field situations is that fractures that are too long to be incorporated into laboratory specimens dominate the response *in situ*. Rice and Rudnicki [48] note that large, partially opened joints or fractures tend to substantially reduce the drained bulk modulus but have little effect on the undrained bulk modulus if they are saturated with liquid water. Consequently, such fractures tend to increase the value of ν_u relative to ν. Since neither ν nor ν_u corresponds directly to values inferred from seismic wave speed ratios [22,49], there appears to be no way of measuring field values directly, although they might be inferred indirectly, for example, from resistivity measurements. Roeloffs [6] does, however, cite an estimate of B of 0.52 to 0.58 inferred for sandstones of the Nubian formation by Beavan *et al* [50] from a combination of laboratory measurements on core samples and studies of well level tidal admittance.

Another approach is based on theoretical estimates of the properties of cracked elastic solids. Rice and Rudnicki [48] tabulate values of ν_u and ν derived from self consistent calculations of [51]. The calculations are for N penny-shaped cracks of radius r per unit volume, so that $\epsilon=Nr^3$ is a crack density. From reported wave speed ratios prior to the 1971 San Fernando earthquake, O'Connell and Budiansky [51] infer values of ϵ in the range of 0.1 to 0.4. For the lower value, ν is reduced to 0.21 from the uncracked value of 0.25 and $\nu_u=0.28$, which gives 1.1 for $(1-\nu)/(1-\nu_u)$, the ratio listed in the last column of Table 1. For $\epsilon=0.4$, ν is reduced to 0.08 and ν_u increases to 0.41 yielding 1.56 for the same ratio.

Values of the diffusivity c (28) control the time scale of fluid mass flow. Again, because long fractures and joints serve as conduits for fluid flow, *in situ* values of the diffusivity are typically much larger than those measured in the laboratory. Roeloffs [6] schematically summarizes values from both laboratory and field data ranging from nearly 10^5 to 10^{-11} m^2/s. For water as pore fluid, $\nu=0.2$ and $G=30$ GPa, values representative of crustal rock, and the second

bracket in Eq. (29) equal to unity, a diffusivity of 1 m/s^2 corresponds to $k=1.25\times10^{-2}$ darcy and $\bar{k}=1.25\times10^{2}$ m/s. The values of k and $\bar{k}$ are reduced by a factor of 10 if $G=3.0$ GPa, listed as representative of gouge in Table 1.

Laboratory values of the diffusivity for the rocks tabulated by [22] are about 10^{-2} to 10^{-4} m^2/s except for the Berea sandstone for which $c=1.6$ m^2/s. Anderson and Whitcomb [52] suggest a value of 1.0 m^2/s as consistent with a variety of earthquake related field phenomena and Rice and Simons [53] argue that this value is consistent with plausible permeabilities and flow rates in fissured rock. Kovach *et al* [54] infer values of 0.01 to 0.1 m^2/s from the response of a well-aquifer system near the San Andreas fault but Roeloffs and Rudnicki [43] suggest that somewhat higher values 1.0 m^2/s are also consistent with their data. From observations of seismicity induced by fluid injection near the Clarendon-Linden fault system in western New York, Fletcher and Sykes [55] estimate diffusivities of 0.5 to 30 m^2/s and Li [56] finds a lower value of 0.1 m^2/s. Li [56] also estimates values of 1.0 to 10.0 m^2/s from seismicity following injection at Matsushiro, Japan. Talwani and Acree [57] estimate 5.0 m^2/s from the rate at which the area of seismicity associated with several reservoirs increased but Roeloffs [6] notes that their approach gives an upper bound. Roeloffs [44] infers diffusivities in the range of 0.01 to 0.26 m^2/s and a lower bound of 0.64 m^2/s from analyses of induced seismicity near Lake Mead, Nevada, and Nurek reservoir, respectively.

A further complication in diffusivity estimates is that the vertical and horizontal values may be significantly different. From data of [58] for a well near the Garlock Fault in California, Rudnicki and Hsu [59] calculate a horizontal diffusivity of 9.3 m^2/s or a value five times larger depending on whether the smaller or larger value of the storage coefficient is used. Lippincott *et al* [58] suggest, however, that the vertical diffusivity is four times larger. By analyzing water level changes due to creep on the San Andreas fault near Parkfield, California, Rudnicki *et al* [60] find values for the horizontal diffusivity of 0.15 m^2/s or 0.06 m^2/s depending on whether the fault is modeled as impermeable or permeable. Analyzing other data from a shallower portion of the same well, Roeloffs *et al* [61] infer vertical diffusivities of 0.03 to 0.04 m^2/s.

In summary, values of diffusivity in the field can vary enormously depending on the location and lithology. The range 0.1 to 1.0 m^2/s does seem representative of conditions near many faults, but values an order of magnitude smaller or larger are not unusual. For the assumptions cited earlier in discussing c (water as pore fluid, $\nu=0.2$ and $G=30$ GPa, and incompressible solid and fluid constituents, corresponding to $B=1$ and $\nu_u=1/2$), this corresponds to k equal to 1.25 to 12.5 md and $\bar{k}$ equal to 0.125 to 1.25 cm/s.

Peltzer *et al* [15] explain observations by SAR of time-dependent strain of the crust following the 1992 Landers, California, earthquake by a relaxation from undrained to drained response over a period of about 273 days. The magnitude of the deformation is consistent with a difference of 0.03 between the undrained and drained values of Poisson's ratio. Since the extent of the deforming region is about 3 km, this length squared divided by the time period gives a diffusivity of 0.38 m^2/s, in the middle of the range inferred above near faults.

4 PLANE STRAIN DISLOCATIONS

The dislocation solutions provide elemental models of shear and opening displacement discontinuities and, hence, are relevant to problems of shear fracture and slippage and tensile fracture in porous media. Superposition of these solutions in time and space can be used to yield more elaborate and realistic slip distributions. Furthermore, the solutions can serve as the basis for numerical formulations of problems with shear or opening discontinuities (*eg*, [62–64]).

4.1 Instantaneous solutions

The basic shear dislocation (gliding edge) corresponds to instantaneous imposition of a uniform discontinuity in the x-direction displacement along the entire negative x-axis:

$$u_x(x,y=0^+)-u_x(x,y=0^-)=b_xH(-x)H(t) \tag{35}$$

The magnitude of the discontinuity is b_x, $H(\ldots)$ denotes the unit (Heaviside) step function and the superscripts $(+)$ and $(-)$ denote limits as $y=0$ is approached through $y>0$ or $y<0$. Figure 2 is a schematic illustration of the geometry. The opening (climbing edge) dislocation corresponds to a discontinuity in the y-direction displacement of magnitude b_y imposed along the negative x axis. The pore pressure change due to sudden imposition of a shear dislocation was first given by [65]. Booker [66] derived the full solution for incompressible constituents and Rice and Cleary [22] give the stress and pore pressure solutions for both shear and opening dislocations in poroelastic materials with compressible constituents.

The pore pressure change induced by an instantaneous shear dislocation is

$$p(x,y,t)=Gb_x\frac{\mu}{2\pi\eta(1-\nu_u)}\frac{y}{r^2}[1-e^{-r^2/4ct}], \tag{36}$$

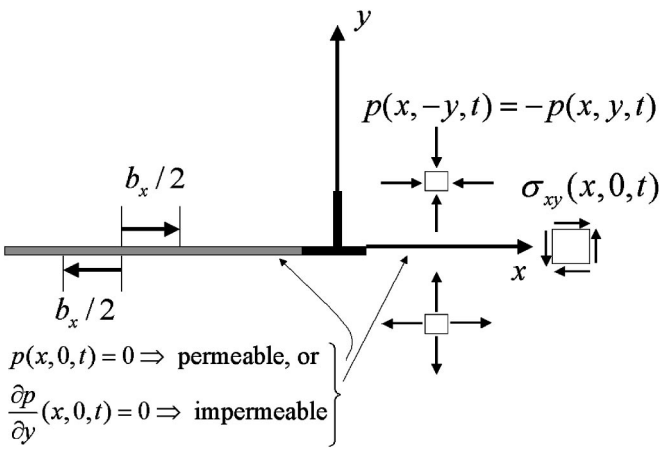

Fig. 2 Shear dislocation corresponding to a discontinuity b_x in u_x on $y=0$, $x<0$; Plane $y=0$ may be permeable ($p=0$) or impermeable ($\partial p/\partial y=0$)

where $r=(x^2+y^2)^{1/2}$. The term outside the square bracket is the undrained solution, obtained in the limit $t\to 0^+$, and the pore pressure decays to zero as $t\to\infty$. Contours of the pore pressure at a fixed time $t\neq 0$ in the half-plane $y\geqslant 0$ are shown in Fig. 3 in the nondimensional form

$$P\left(\frac{x}{\sqrt{4ct}},\frac{y}{\sqrt{4ct}}\right)=\frac{2\pi(1-\nu_u)\eta}{\mu G}\frac{\sqrt{4ct}}{b_x}p(x,y,t). \tag{37}$$

The shear stress change on the slip plane ($y=0$) is

$$\sigma_{xy}(x,0,t)=\frac{Gb_x}{2\pi(1-\nu_u)}\left\{1-\mu F_p\left[\frac{4ct}{x^2}\right]\right\} \tag{38}$$

where

$$F_p(T)=T[1-\exp(-1/T)]. \tag{39}$$

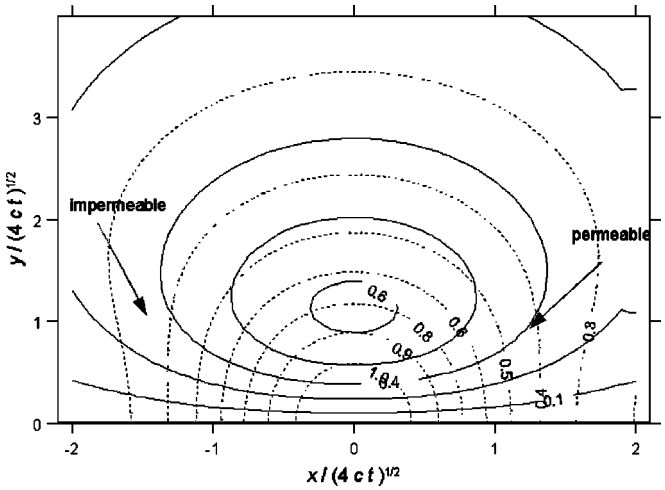

Fig. 3 Contours of pore pressure in the nondimensional form (37) induced by a shear dislocation on permeable (solid) and impermeable (dashed) plane; contours are for a fixed time not equal to zero

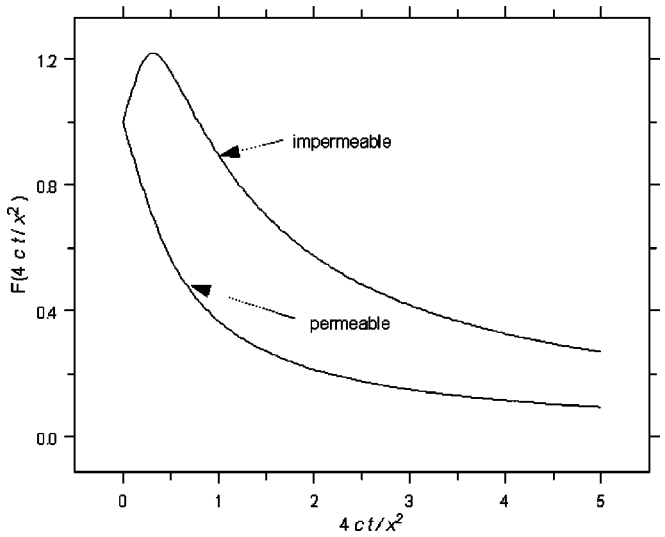

Fig. 4 Time variation of the shear stress induced by a shear dislocation on a permeable and impermeable plane

As in Eq. (36), the first term is the undrained response and $F_p\to 0$ as $T\to 0$. For long times, F_p approaches unity and the bracket $\{\ldots\}$ in (38) becomes $1-\mu=(1-\nu_u)/(1-\nu)$. As noted earlier, this ratio is a measure of the magnitude of porous media effects. The decay in time of $\sigma_{xy}(x,0,t)$ (at a fixed x) from the undrained value to the drained value is given by the function F_p which is plotted in Fig. 4.

As is evident from the expression (36), the pore pressure vanishes on $y=0$. This feature is a consequence of the antisymmetry and continuity of the pore pressure about $y=0$. The derivative of the pore pressure in the y direction does not, however, vanish on $y=0$ and is plotted in nondimensional form in Fig. 5. From Darcy's law (21), this implies that fluid mass flows across the slip plane. Many faults in the Earth's crust are thought to be barriers to fluid flow across the fault plane because of the presence of clay particles [67,68], the fabric that has developed from past shearing and the absence of fractures traversing the fault plane. (Faults may, however, be conduits for flow along the fault). Consequently, the solution for a shear dislocation on an impermeable plane may be more appropriate for application to faults. If the plane $y=0$ is impermeable then

$$\partial p/\partial y=0 \tag{40}$$

there, but the pore pressure is no longer required to be continuous. The condition (40) and a discontinuous pore pressure idealize a thin shear zone of impermeable material. Rudnicki [69] derived the stress and pore pressure fields for a shear dislocation on an impermeable plane. The pore pressure change is

$$p(x,y,t)=-\frac{Gb_x\mu}{2\pi\eta(1-\nu_u)}\mathrm{Im}\left\{1-\mu\frac{W(x,y,t)}{\xi}\right\}, \tag{41}$$

where $\xi=x+\iota y$, $\iota=\sqrt{-1}$, $\mathrm{Im}\{\ldots\}$ denotes the imaginary part of $\{\ldots\}$, and

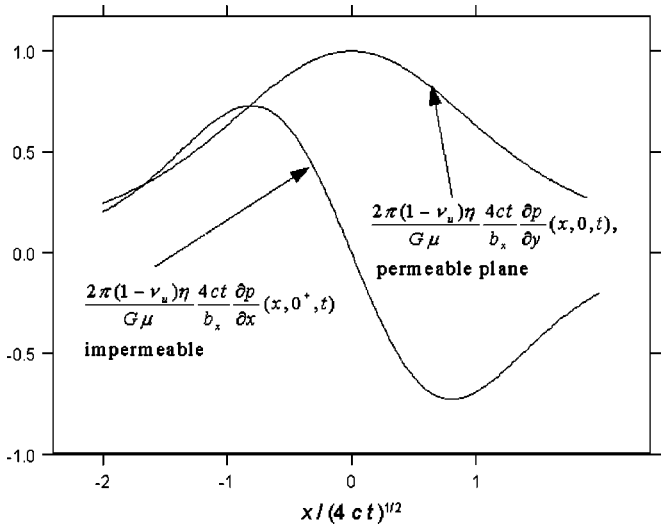

Fig. 5 Pore pressure gradient (proportional to negative of fluid mass flux) on $y=0$ in the y direction for a shear dislocation on a permeable plane and in x direction for a shear dislocation on an impermeable plane

$$W(x,y,t)=\operatorname{erfc}\left\{\frac{y}{\sqrt{4ct}}\right\}+\exp\left[\frac{-r^2}{4ct}\right]\operatorname{erf}\left\{\frac{\iota x}{\sqrt{4ct}}\right\}. \tag{42}$$

Alternatively, the second term of Eq. (42) can be expressed in terms of Dawson's integral [70]

$$\mathrm{D}(x)=\exp(-x^2)\int_0^x \exp(t^2)dt \tag{43}$$

as

$$W(x,y,t)=\operatorname{erfc}\left\{\frac{y}{\sqrt{4ct}}\right\}+\frac{2\iota}{\sqrt{\pi}}\exp\left[\frac{-y^2}{4ct}\right]\mathrm{D}\left\{\frac{x}{\sqrt{4ct}}\right\}. \tag{44}$$

The expression (41) gives the pressure for $y\geqslant 0$; for $y\leqslant 0$, the pore pressure is equal in magnitude and opposite in sign. The maximum pore pressure change is on $y=0$ for the impermeable plane but diffuses away from $y=0$ with time for the permeable plane. Contours of the pore pressure (at a fixed time not equal to zero) are shown in Fig. 3 in the same nondimensional form as in (37). The contours coincide with those for the shear dislocation on a permeable fault away from $y=0$, but intersect $y=0$ at right angles, as required by the condition (40). The pore pressure induced on $y=0^+$ is plotted in Fig. 6; the pore pressure on the negative side of $y=0$ is equal in magnitude and opposite in sign. Although the boundary condition (40) requires that $\partial p/\partial y=0$ on $y=0$, $\partial p/\partial x\neq 0$ there and is plotted in nondimensional form in Fig. 5. Thus, there is fluid mass flow along the fault plane in response to the induced variation of pressure.

The shear stress on the dislocation plane has the same form as (38) but the function expressing the time dependence is given by

$$F_i(T)=2e^{-1/T}-T(1-e^{-1/T}) \tag{45}$$

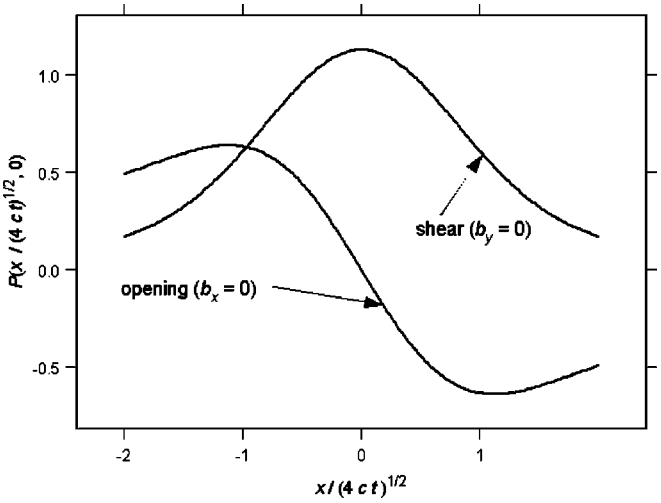

Fig. 6 Pore pressure (in nondimensional form) induced on an impermeable plane $y=0$ by a shear dislocation and an opening dislocation. The pore pressure is continuous across $y=0$ for the opening dislocation but discontinous for the shear dislocation. Values on $y=0^-$ for the shear dislocation are equal magnitude and opposite in sign to those shown.

The function F_i has the same limits as Eq. (39). But, in contrast to the solution for the permeable plane, the shear stress does not decay monotonically with time from the larger undrained value to the drained value. Instead, the shear stress first rises from the initial undrained value about an additional 20% of the difference between the undrained and drained values at $4ct/x^2\approx 0.3$ and then decays to the drained value (Fig. 4). Rudnicki [69,71] give various plots of the pore pressure, pore pressure gradients on $y=0$, and the shear stress.

Rice and Cleary [22] also give the solution for an opening dislocation. In this case, symmetry of the problem and continuity of the pore pressure and its gradient require (40) on $y=0$. The pore pressure induced on $y=0$ is plotted in Fig. 6. Rudnicki [71] derives the full stress field for an opening dislocation on a permeable plane, idealizing a narrow region in which the permeability in the x-direction is so large that any pore pressure alterations are rapidly equilibrated. For this solution $p=0$ is enforced on $y=0$, but $\partial p/\partial y$ is discontinuous and non-zero on $y=0$. Consequently, there is a net flux of fluid mass to this plane. Surprisingly, the time dependences of the normal traction (σ_{yy}) for opening dislocations on impermeable and permeable planes are also given by (45) and (39), respectively.

4.2 Steadily moving solutions

Solutions for steadily moving dislocations can, in principle, be obtained by integration of the instantaneous solutions, but are more easily established by direct solution of the governing equations. Rudnicki and Roeloffs [72] use Fourier transform methods to give the complete stress and pore pressure fields for shear dislocations moving steadily on permeable and impermeable planes. The pore pressure induced by the dislocation on the permeable plane is

$$p=\frac{\mu}{\eta}\frac{Gb_x}{4\pi(1-\nu_u)}\left\{1-\frac{Vr}{2c}e^{-Vx/2c}K_1\left(\frac{Vr}{2c}\right)\right\} \tag{46}$$

and on the impermeable plane is

$$p=\pm\frac{\mu}{\eta}\frac{Gb_x}{4\pi(1-\nu_u)}\frac{V}{c}e^{-Vx/2c}\int_{-\cos\theta}^{1}\frac{1+u\cos\theta}{\sqrt{1-u^2}}e^{-Vr/2c\,u}du \tag{47}$$

where V is the speed, x is now measured from an origin moving with the dislocation, $\theta=\arctan(y/x)$, $K_1(s)$ is the modified Bessel function of order one [70], and the upper and lower signs apply for $y>0$ and $y<0$, respectively. The expression (47) vanishes identically for $y=0$, $x<0$ and is discontinuous at $x=0$. Thus, both p and $\partial p/\partial y$ vanish on $y=0$ for $x<0$. The behavior as $r\to 0$ is

$$p=\frac{\mu}{\eta}\frac{Gb_x}{4\pi(1-\nu_u)}\frac{V}{c}\left\{\pi-\theta+\frac{1}{2}\sin(2\theta)\right\} \tag{48}$$

An interesting feature of (46), noted by [43] is that the pore pressure change reverses sign in a wake trailing the dislocation. This reversal does not occur for the impermeable plane.

Figure 7 shows the pore pressure (in nondimensional form, $4\pi p(1-\nu_u)\eta/G\mu(Vb_x/c)$) as a function of the nondimensional time V^2t/c induced by dislocations moving

steadily on a permeable (dashed) and an impermeable (solid) plane. Results are shown for two nondimensional distances $Vy/2c$ from the fault plane, 0.1 and 1.0 and $t=0$ is the time at which the dislocation is closest to the observation point. For $V=1$ km/day and $c=1$ m^2/s, $2c/V=172.8$ m and $c/V^2=2.07$ hours. Figures 8 and 9 show contours of the nondimensional pore pressure (in nondimensional coordinates moving with the dislocation) for dislocations moving steadily on a permeable (Fig. 8) and an impermeable (Fig. 9).

The shear stress induced on $y=0$ by the shear dislocation can be written in the form

$$\sigma(x,y=0)=\frac{Gb_x}{2\pi(1-\nu_u)}\{1-\mu g(Vx/c)\}, \tag{49}$$

where the term on the right hand side outside the bracket is the usual elasticity solution with the undrained Poisson's ratio. The function $g(Vx/c)=0$ for large values of its argument and is unity when its argument is zero. Thus, the expression for the shear stress varies between the undrained and drained elasticity solutions. For the shear dislocation on a permeable plane Cleary [62] obtained an expression for $g(Vx/c)$ in integral form and evaluated it numerically and Simons [73] gave the following analytic expression in terms of the modified Bessel function K_1 [70]:

$$g(z)=\frac{1}{z}\{1-|z|e^{-z}K_1(z)\} \tag{50}$$

Rudnicki and Roeloffs [72] derived expressions for the full stress and pore pressure fields for shear dislocations moving steadily on both permeable and impermealbe planes. The expression for g for the impermeable plane is

$$g(z)=4z\int_1^\infty u\left(\sqrt{\frac{u}{u-1}}-1\right)e^{-2zu}du-\frac{1}{z}(1-e^{-2z})+2e^{-2z},\quad z\geqslant 0 \tag{51a}$$

$$=\frac{3}{2|z|}\int_0^\infty\frac{(1-e^{-2|z|u^2})}{(1+u^2)^{5/2}}du,\quad z<0 \tag{51b}$$

These expressions are given in a different form, more convenient for numerical evaluation, than those in [72]. (Also, note that the lower limit of the integral in the expression for $g(z)$, $z<0$, in Eq. (55) of [72] should be zero not unity). The functions g are plotted for both the permeable and impermeable faults in Fig. 10. Both functions slightly exceed unity, the drained value, for small positive values of the argument (slightly ahead of the dislocation). This effect will, however, be overwhelmed by the x^{-1} behavior in the full expression for the shear stress on $y=0$ (49). The graph of g for the shear dislocation on an impermeable plane appears to be identical with the result of [62] given in graphical form, for the normal traction on the plane of an opening dislocation moving steadily on $y=0$. Thus, the relation between shear and opening dislocations on permeable and impermeable planes that applies for the instantaneous case may also apply for steady state motion.

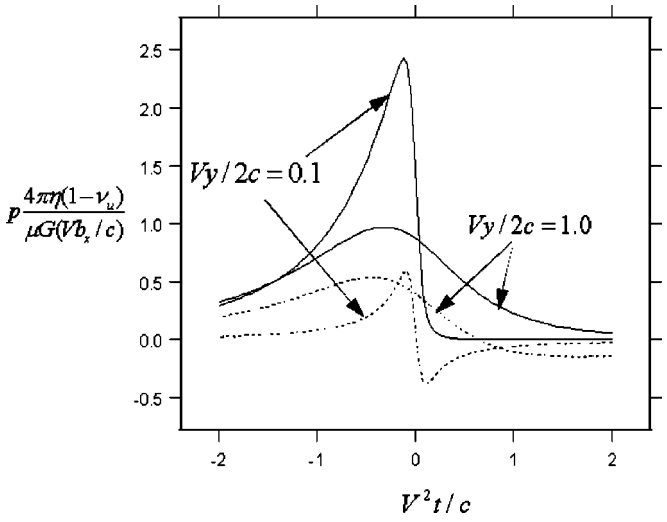

Fig. 7 Pore pressure (in nondimensional form) *vs* the nondimensional time V^2t/c for dislocations moving steadily on permeable (dashed) and impermeable (solid) planes

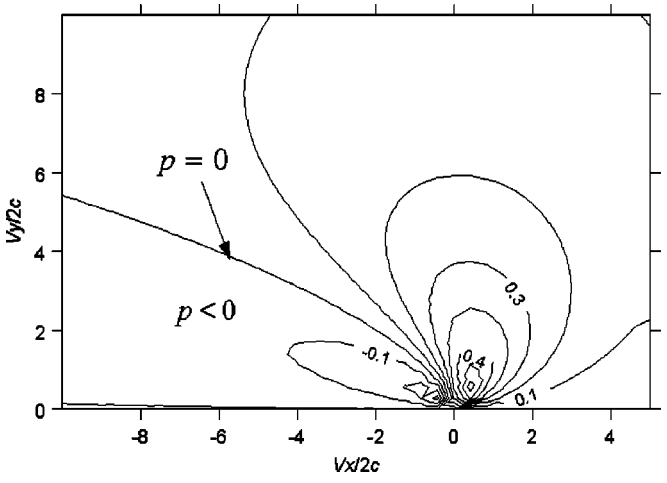

Fig. 8 Contours of nondimensional pore pressure for a shear dislocation moving steadily on a permeable plane

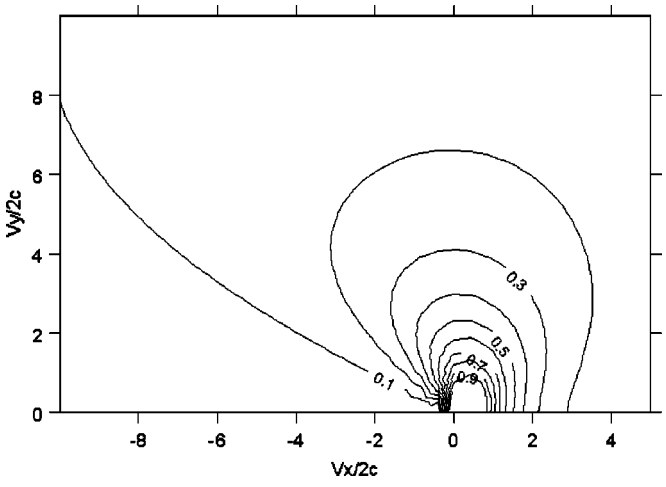

Fig. 9 Contours of nondimensional pore pressure for a shear dislocation moving steadily on an impermeable plane

4.3 Applications to fault processes

One application of the shear dislocation solutions just described is to water well level changes induced by creep events on faults in the Earth's crust. Creep events are slip events that move too slowly, typically in the range of 1 to 10 km/day, to excite seismic waves. Water wells can act as sensitive indicators of volumetric strain, responding to changes of the order of 10^{-8}. Although local site conditions may complicate the response, the response to earth tides (*eg,* [6]) can be used to calibrate the well.

Rudnicki *et al* [60] found that the pore pressure distributions due to simple dislocations, Eqs. (36) and (41) were sufficient to describe water level changes induced in a well by creep on the San Andreas fault near Parkfield, California. Figure 11 schematically illustrates the position of the water well and two creepmeters. Because the distance of the well from the fault is known (460 m), comparison of the observed water well level changes with the predicted pore pressure changes were used to infer the magnitude of the slip and the distance northwest of the well that the slip stopped. (For this well and the frequency of these observations, pressure change is approximately equivalent to change in static head of the water level). The inset in Fig. 11 shows the pore pressure predicted from Eqs. (36) and (41), divided by the values at $t=0$, against the nondimensional time $4ct/(460\ \mathrm{m})^2$. Results are shown for two values of the angle θ, 55° and 90°, that Rudnicki *et al* [60] found bracketed the observations. The inferences for the magnitude and position of the slip were consistent with slip measured at the surface on creepmeters northwest and southeast of the well for three of the five events analyzed. Discrepancies in the remaining two events suggested that the surface slip measured by the creepmeters differed significantly from that near the 240 m depth of the well.

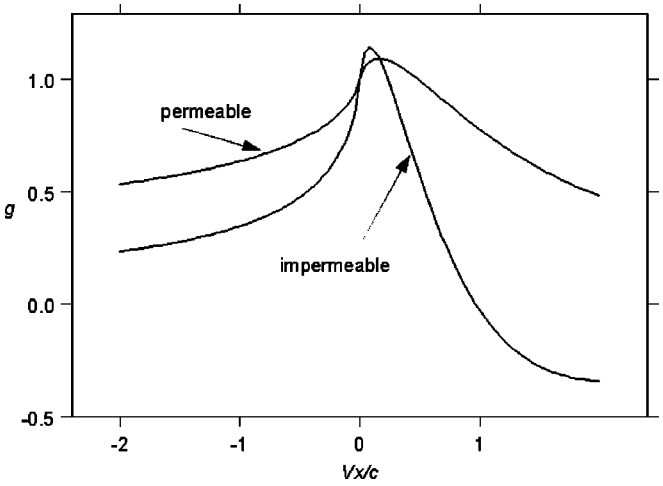

Fig. 10 The functions g (49) for the shear stress on $y=0$ for a shear dislocation moving steadily on a permeable and an impermeable plane

Rudnicki and Hsu [59] used two dislocations of opposite sign separated by a distance $2L$ to model a finite length slip zone and examined the pore pressure change induced by a ramp increase in time of the slip magnitude (Fig. 12). They used these solutions to interpret water well level changes due to creep events near the Garlock Fault (California) observed by [58]. Their solution including coupled deformation diffusion describes the observed water-well level changes as well as that of [58] who neglect these effects but use a more complex spatial distribution of propagating slip. The magnitude of the slip inferred by [59] is not well constrained by the data but includes the 0.5 to 1.0 cm range inferred by [58].

Roeloffs and Rudnicki [43] use Eq. (46) and superposition of this result for an exponential distribution of slip to examine coupled deformation diffusion effects on water level changes. They compare a model of a water level change observed by [74] based on (46) with a purely elastic model by [75]. Agreement with the observations is similar for the

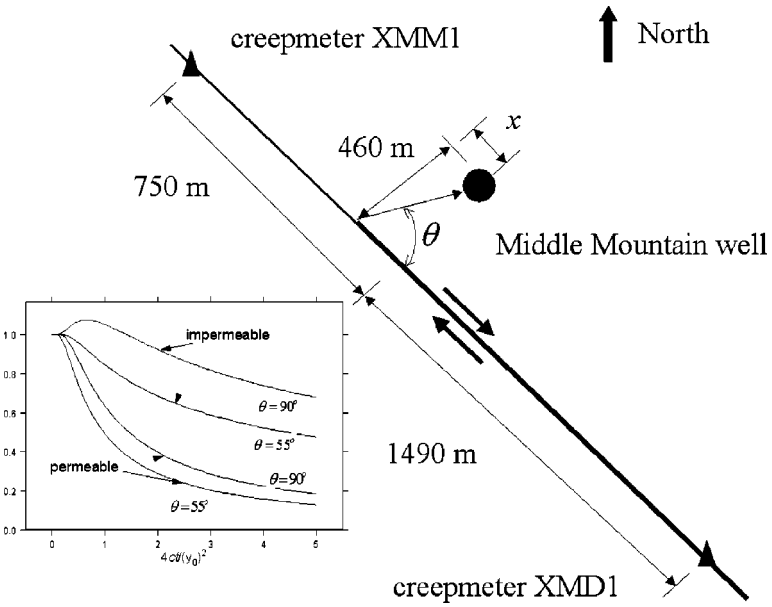

Fig. 11 Schematic illustration of the position of the Middle Mountain water well and creepmeters near the San Andreas fault near Parkfield, California. The inset shows the predicted pressure changes (divided by the instantaneous change) against $4ct/(460\ \mathrm{m})^2$.

two models, but uncertainties in parameters prevent a definite conclusion about whether coupled deformation diffusion effects are significant in this particular case.

Rudnicki [36] summarizes the pore pressure solutions for moving and stationary shear dislocations and uses superposition to calculate the pore pressure changes for non-steadily moving shear dislocations on a permeable fault. In particular, he presents numerical results for dislocations that start from rest, move at a constant speed and stop, compares them to the instantaneous and steadily moving solutions, and identifies ranges of parameters where the simpler solutions suffice. Although these more elaborate solutions are likely better representations of actual slip events, observations are seldom sufficiently dense to distinguish details of the different solutions.

All the solutions discussed here are 2D (plane strain). To date observations of water well level changes have not been sufficient to constrain adequately the shape of slip zones for 3D solutions. Rudnicki [36] has, however, noted that the instantaneous and steadily moving solutions can be interpreted as different limiting idealizations of 3D slip events. As illustrated in Fig. 13*a*, a slip event of magnitude Δ that is propagating vertically with a speed V may be observed at the same time at two points at the same depth as a ramp with rise time Δ/V. On the other hand, as illustrated in Fig. 13*b* an event that is propagating mainly parallel to the surface may be observed at two points at the same depth as steadily propagating with speed V.

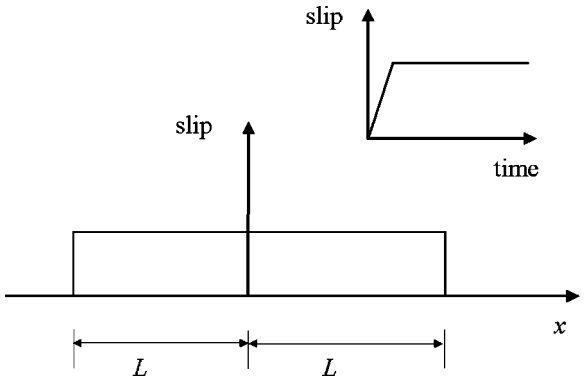

Fig. 12 Slip distribution created by two dislocations of opposite sign at $x=\pm L$ and the ramp time function used by Rudnicki and Hsu [59] to analyze pore pressure changes due to slip

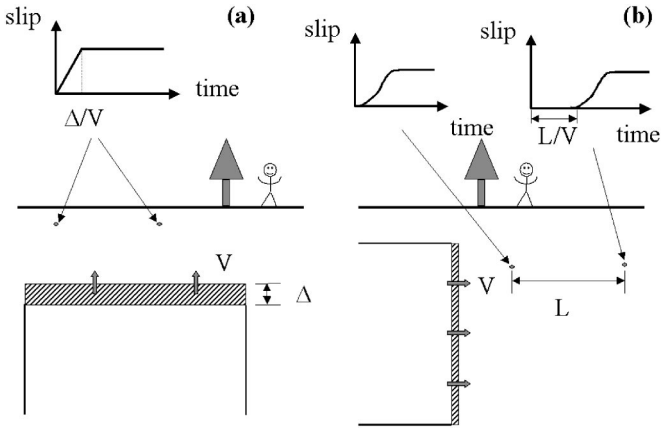

Fig. 13 Cartoon illustrating that the stationary dislocation with a ramp time function used by [59] and the steady-state solutions used by [43] can be interpreted as limiting cases of 3D solutions

In order to estimate the effect of flow to a free surface, Rudnicki and Wu [76] have used the solution of the 1D version of Eq. (27), without body forces but with a source term $Q(y,t)=Q_0\delta(y-d)\delta(t)$, where $\delta(\ldots)$ is the Dirac delta function. If σ_{yy} is constant, then the solution for the pore pressure is

$$p(y,t)=\frac{Q_0}{(\kappa/c)\rho_0}\frac{\exp[-(y-d)^2/4ct]}{\sqrt{4\pi ct}}. \tag{52}$$

Adding an image source of strength $-Q_0$ at $y=-d$ leaves the surface $y=0$ free of pore pressure. Rudnicki and Wu [76] used this solution to help interpret the effect of flow to a free surface in a 2D finite element solution for pore pressure changes due to buried slip in a half space. Although the effect depends on the spatial distribution of the source, they find, roughly, that the effect of the free surface is not significant for $t<0.5d^2/4c$ and $y>d$. As an example, Fig. 14 compares the full-space (dashed lines) and half-space solutions at depths 20%, 50%, and 75% of the distance from the free surface to the source with the full space solution at the same distance from the source. Obviously, the effect of the free surface occurs at later times for deeper positions. The finite element solution reveals an additional effect: The volume strains are larger near the free surface than they would be in a half space; consequently, the pore pressure changes near the free surface are initially greater than for the full space (at the same distance from the slip zone) but the proximity of the free surface causes the pore pressures to decay more rapidly.

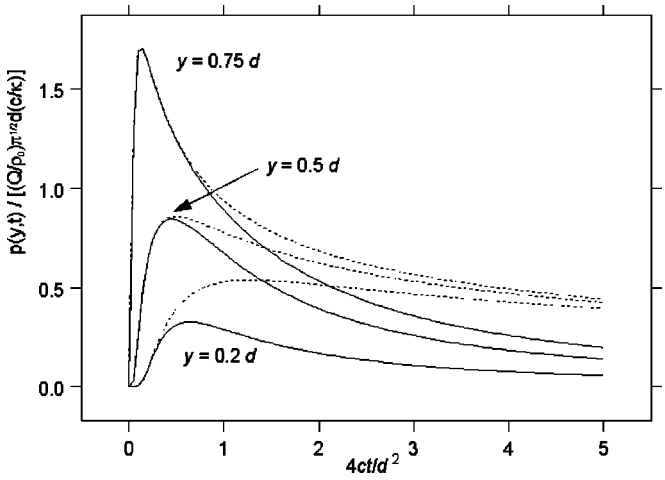

Fig. 14 Pore pressure, divided by $Q_0c/\sqrt{\pi}d\rho_0\kappa$, due to an instantaneous injection of fluid mass per unit area Q_0 at a depth d. Curves compare the solution for the halfspace (solid) at three different depths with the full space solution (dashed) at the same distance from the source.

Nur and Booker [65] suggested that the pore pressure changes (36) could contribute to the occurrence of aftershocks, which are smaller earthquakes following a larger one. Booker [66] noted that since the stress drop (38) on the slip plane decays with time, the total stress on the slip plane increases. This provides a time-dependent mechanism for reloading the fault and could also contribute to aftershocks. Applications of the shear dislocation solution to aftershock processes are also discussed by [22] and [77]. Rudnicki [69] discusses modifications of these results for the case of a shear dislocation on an impermeable plane.

The application of the dislocation solutions discussed thus far has been purely kinematic; that is, the distribution and evolution of slip is specified. Generally, in applications to fault mechanics the slip is unknown, evolves in response to far field loads, and the evolution depends on the relation between the shear stress on the fault surface, τ_{flt}, and the relative displacement, that is, the slip δ, and its past history. As outlined by [22], superposition of dislocations in space and time and specification of the relation between τ_{flt} and δ leads to a nonlinear integral equation for the evolution of slip in response to increasing far field loads. Rudnicki [78] used this approach to study the stabilization of slip on a fault surface by coupled deformation-diffusion effects. He assumed the shear stress depended only on the slip (not on its velocity or past history) and that the τ_{flt} versus δ relation is parabolic near peak. Furthermore, he idealized the spatial distribution of slip as a boxcar: dislocations of opposite sign a distance $2L$ apart (see Fig. 12). Because the τ_{flt} *versus* δ relation has a negative slope (as, for example, in Fig. 17*b*), an inertial instability is possible if shear stress on the fault decreases more rapidly than the surrounding material can unload. For slow slip (relative to the time scale of diffusion), the material surrounding the fault behaves in more compliant drained fashion, but stabilization occurs because the surrounding material responds more stiffly as slip on the surface accelerates. If, however, the τ_{flt} *versus* δ relation continues to decrease, instability occurs in the limit as the surrounding material approaches undrained response. Rudnicki [78] calculates precursory times, defined as the difference between the time instability occurs and when it would have occurred in the absence of coupled-deformation diffusion effects. For representative parameters, precursory times are short, less than a day or two. Koutsibelas [79] performs analagous calculations for an impermeable fault, a cubic τ_{flt} *versus* δ relation, and an elliptical distribution of slip. Precursory times are similar but shorter for the cubic distribution of slip than the parabolic. Precursory times slightly longer for the impermeable fault and for the elliptical distribution of slip. Rice and Rudnicki [48] calculated much longer precursory times, 10 to a few hundred days, for the same mechanism based on a solution for a spherical inclusion in a poroelastic solid, but modified to approximate narrow fault-like zones. Although this mechanism may contribute to processes preceding some earthquakes, rate and state dependent effects associated with the friction relation itself are thought to be more significant (eg, [80]).

5 STABILIZATION OF SPREADING SHEAR CRACKS

Because rapid deformation of a poroelastic solid evokes the stiffer undrained response, rapid crack propagation requires a larger driving force than slow propagation. This stabilizing effect has been examined in detail by [53] and applied to spreading shear faults (Fig. 15*a*). They solved the problem of a semi-infinite crack propagating steadily at a speed V in a porous elastic solid. A stress drop, $\tau_\infty - \tau_f$, representing the difference between far field loads and a uniform frictional resistance was applied over a finite distance l behind the crack-tip in order to simulate a finite length fracture (Fig. 15*b*). Rice and Simons [53] show that the shear stress near the crack-tip has a spatial distribution identical to that in an ordinary elastic solid [81] but the stress intensity factor is given by

$$K = K_{nom} h(Vl/c) \tag{53}$$

where $K_{nom} = (\tau_\infty - \tau_f)(8l/\pi)^{1/2}$. The function $h = 1$ at $V = 0$ and decreases monotonically to $(1-\nu_u)/(1-\nu)$ as $V \to \infty$. The energy released per unit area of crack advance $\mathcal{G}$ is related to K by

$$\mathcal{G} = K^2(1-\nu)/2G \tag{54}$$

If crack propagation is assumed to occur at a critical value of energy release rate $\mathcal{G}_{crit}$, the substitution of (53) into (54) yields

$$\mathcal{G}_{nom}/\mathcal{G}_{crit} = [h(Vl/c]^{-2} \tag{55}$$

where $\mathcal{G}_{nom} = K_{nom}^2(1-\nu)/2G$ is the energy required to drive the crack at a speed V in an ordinary elastic solid. Thus, Eq. (55) indicates the energy required to drive the crack in a poroelastic solid increases with speed and the ratio (55) ap-

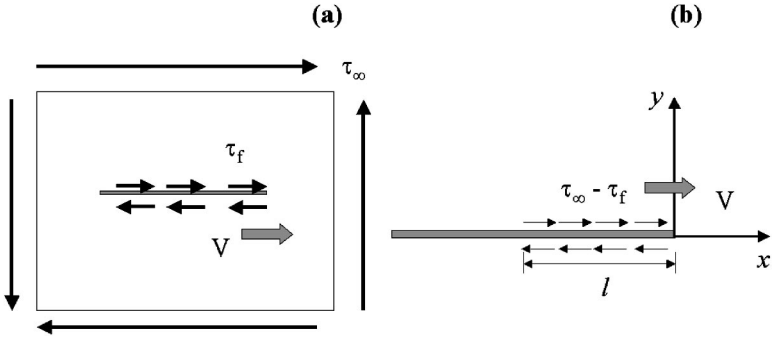

Fig. 15 Idealizations of a propagating shear fault: *a*) Finite length fault loaded in the farfield with a uniform shear stress τ_∞ and having a uniform resistive friction stress τ_f. *b*) Stress difference $\tau_\infty - \tau_f$ is applied a distance l behind the edge of a semi-infinite fault in order to simulate a finite fault.

proaches maximum of $[(1-\nu)/(1-\nu_u)]^2$ as $V\to\infty$. The square root of this factor is listed for various rock types in Table 1.

In the solution of [53], the pore pressure vanishes identically on the crack plane, and, as discussed for the dislocation solutions, this corresponds to a permeable shear fault. Rudnicki and Koutsibelas [82] examine the analogous problem for the impermeable plane. The results are similar but the ratio $\mathcal{G}_{nom}/\mathcal{G}_{crit}$ rises more rapidly for the impermeable plane than the permeable. Curves of $\mathcal{G}_{nom}/\mathcal{G}_{crit}$ against Vl/c are shown in Figure 16 for both permeable (dashed) and impermeable (solid) planes for several values of $(1-\nu)/(1-\nu_u)$, 1.14, 4/3, 3/2, and 5/3. The first two correspond to the entries of *rock* and *gouge* in Table 1; the last two are more representative of soils.

A limitation of these results is that the idealization of a singular stress at the crack edge is appropriate only if the size scale of actual inelastic processes near the edge is much smaller than any characteristic length in the problem. For large speeds, the characteristic diffusion length c/V becomes small and approaches zero as $V\to\infty$. To overcome this limitation, Rice and Simons [53] incorporate a cohesive zone (Fig. 17) of higher frictional resistance $\tau_B > \tau_f$ over a distance $\omega < l$ behind the crack edge (where the relative slip displacement falls to zero). This is intended as an idealization of a more elaborate endzone model in which the shear stress depends on the relative slip (or even slip-rate and history). The propagation criterion now becomes that the slip at the back edge of the cohesive zone equals a critical value δ_{crit}. The size of the cohesive zone should be determined so that the stress at the crack edge is finite, but Rice and Simons [53] find that the variation of ω with δ_{crit} is small, and, because of the cost of the numerical calculations, they give results for fixed values of ω/l.

When the cohesive zone is included, the propagation criterion can still be phrased in the form (55), but this ratio now does not increase monotonically with speed. Instead, it rises to a value that approaches $[(1-\nu)/(1-\nu_u)]^2$ for small endzone sizes, but then falls to a limiting value of $(1-\nu)/(1-\nu_u)$ as $V\to\infty$. For the impermeable fault plane, Rudnicki and Koutsibelas [82] find that $\mathcal{G}_{nom}/\mathcal{G}_{crit}$ reaches a slightly higher peak at a slightly lower value of Vl/c. For example, for $\omega/l = 10^{-3}$, and $(1-\nu)/(1-\nu_u) = 4/3$, the peak of $\mathcal{G}_{nom}/\mathcal{G}_{crit} = 1.76$ at about $Vl/c = 10^2$ for the impermeable fault and 1.69 at $Vl/c = 10^3$ for the permeable. For both permeable and impermeable planes, there is a finite range of Vl/c in which the energy required to drive the crack increases with speed. The maximum value of Vl/c for stabilization is about 10^3 to 10^4. Rice and Simons [53] note that for speeds of typical creep events, 1 to 10 km/day, $c = 1\ \mathrm{m}^2/\mathrm{s}$ and l from 0.1 to 10 km, Vl/c ranges from 1 to 10^3. Thus, the stabilizing effects of coupling between deformation and diffusion provide a possible mechanism for the occurrence of creep events.

To first order, the frictional resistance on a shear fault or frictional surface is given by the Coulomb stress

$$\tau_c = \tau_f + f\overline{\sigma}_n, \tag{56}$$

where τ_f is the cohesion, f is a friction coefficient, $\overline{\sigma}_n$ is the effective compressive stress on the surface. For slip on frictional surfaces, experiments [83] and theory [84] indicate that the appropriate form for $\overline{\sigma}_n$ is the difference between the total compressive stress and the pore fluid pressure. For the shear crack on an impermeable plane, anti-symmetry and continuity of the normal stress and pore pressure require that both vanish and, hence, the Coulomb stress (56) reduces to τ_f, assumed to be uniform. For the shear crack on an impermeable plane, the same considerations require the normal stress to be zero; the pore pressure is, however, non-zero, though still anti-symmetric and, hence, has values equal in magnitude and opposite in sign as the plane is approached from above or below. Although it might be thought that the net effect of the equal and opposite pore pressures cancel, Rudnicki and Koutsibelas [82], following a suggestion of Rice (personal communication, 1987), argue that it is the

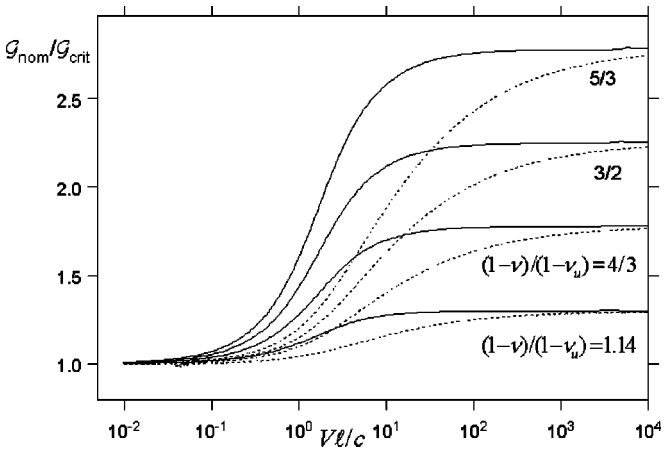

Fig. 16 Curves of $\mathcal{G}_{nom}/\mathcal{G}_{crit}$ against Vl/c for four values of the ratio $(1-\nu)/(1-\nu_u)$. For large values of Vl/c, $\mathcal{G}_{nom}/\mathcal{G}_{crit}$ approaches the square of this ratio. Dashed curves are for permeable and solid for impermeable.

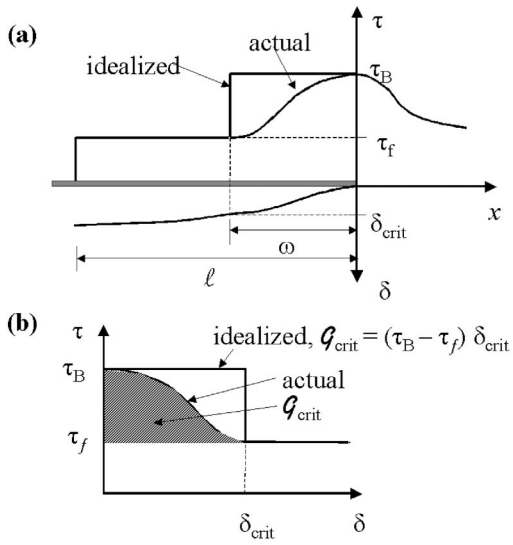

Fig. 17 Sketch illustrating the cohesive zone model *a*) used by [53] and the shear stress *versus* slip relation *b*)

pore pressure increase that is relevant to propagation: the slip plane idealizes an impermeable zone of small but finite thickness and the discontinuity in pore pressure idealizes a sharp gradient across the narrow zone; because the effective compressive stress and, hence, the frictional resistance, decreases with a pore pressure increase, the slip will tend to localize in the portion of the fault zone where the pore pressure increase is greatest. Based on this assumption, Rudnicki and Koutsibelas [82] calculate the destabilizing effect of the pore pressure increase on propagation. For simplicity, they obtain the distribution of pore pressure by superimposing the solution for the pore pressure due to a shear dislocation on an impermeable plane [72] and assume a distribution of slip in the endzone given by the purely elastic solution. The resulting pore pressure change increases from slightly ahead of the edge of the slip zone to a maximum near the back of the endzone, but the distribution narrows sharply with increasing Vl/c. Because the increase in pore pressure is destabilizing, $\mathcal{G}_{nom}/\mathcal{G}_{crit}$ is less than unity. But, because of the narrowing of the pore pressure distribution, $\mathcal{G}_{nom}/\mathcal{G}_{crit}$ decreases with Vl/c until values of about $10^{1/2}$ and then increases slowly. Estimates for plausible parameters suggest that the pore pressure change can be a significant fraction, perhaps, 40 to 70%, of the driving stress.

Rice and Simons [53] rationalize the result (53) by noting that the vicinity of the propagating edge acts as a drained inclusion in an undrained matrix. Simons [85] elaborates on this interpretation by using matched asymptotic expansions for a propagating shear crack in a poroelastic material. He finds that at high speeds of propagation the transition from an inner drained region to an outer undrained region occurs in boundary layers near the crack-tip and crack faces and he obtains closed-form expressions for the stresses and pore pressure in these regions. Rudnicki [86] performs an analogous boundary layer analysis for the shear crack on an impermeable plane. In contrast to the pore pressure solution for the shear crack on the permeable plane, which vanishes along all rays approaching the crack-tip, Rudnicki [86] finds that the pore pressure approaches a constant value for the impermeable plane if the crack-tip is approached from above. The value is equal in magnitude and opposite in sign if the crack tip is approached from below. Because the crack-tip pore pressure is bounded while the stresses become singular as the square root of distance from the crack-tip, the near-tip region is effectively drained for the impermeable crack as well as for the permeable even though the pore pressure change for the impermeable plane is non-zero and discontinuous.

In the problem considered by Rice and Simons [53], the entire crack plane, both ahead and behind the moving edge, is considered permeable and, hence, the pore pressure is zero everywhere on $y=0$. Similarly, Rudnicki and Koutsibelas [82] enforce the condition $\partial p/\partial y=0$ everywhere on the crack plane. Alternatively, it might be argued that symmetry and continuity of pore pressure require $p=0$ ahead of the propagating crack but the crack faces are permeable, corresponding to $p=0$, or impermeable, corresponding to the condition $\partial p/\partial y=0$, behind the crack edge. The latter problem has been solved by Craster and Atkinson [87,88]. Interestingly, the asymptotic behavior as the crack-tip is approached is identical to that found in [85].

Ruina [89] has solved the problem of a tensile crack propagating in the porous elastic material and notes that the stabilizing effects may contribute to the retardation of hydraulic fractures. Ruina [89] enforces the condition, $\partial p/\partial y=0$, implied by symmetry and continuity of fluid mass flux, everywhere on the crack plane, but Atkinson and Craster [90] consider the possibility that the crack faces are permeable and, hence, $p=0$ there. Atkinson and Craster [90] and Craster and Atkinson [87,88,91] consider a number of other problems of stationary and steadily moving tensile and shear cracks. A summary of their results is given in [92]. Cleary [62] has used superposition of the solution of steadily moving shear and opening dislocations and fluid mass sources to formulate integral equations for steadily moving fractures. He solves these equations numerically for several examples and discusses applications of the results to tensile and shear fractures.

6 INCLUSION MODELS

Reservoirs, aquifers, fault zones and other inhomogeneities have different material properties and/or pore pressure than the surrounding material. If the inhomogeneity is not too close to a free surface, it can be regarded as embedded in an infinite linear elastic matrix. If, in addition, the shape of the inhomogeneity can be approximated as ellipsoidal, then the results of [93] can be used to constrain the response of the inhomogeneity to far field stresses or strains or changes in pore pressure or fluid mass. Eshelby [93] showed that the boundary of an ellipsoidal inclusion in an infinite elastic matrix subjected to far field stress or strain deforms in a manner consistent with uniform strain of the interior. Consequently, the stress and strain in the inhomogeneity, σ_{ij}, ε_{ij}, are related to the far field stress and strain σ^{∞}_{ij}, $\varepsilon^{\infty}_{ij}$ by

$$S_{mnkl}C_{klij}\{\sigma_{ij}-\sigma^{\infty}_{ij}\}=\{S_{mnkl}-\delta_{mk}\delta_{nl}\}(\varepsilon_{kl}-\varepsilon^{\infty}_{kl}) \qquad (57)$$

where C_{klij} is the tensor of elastic compliances of the surrounding material and the S_{mnkl} are an array of factors given in [93]. The S_{mnkl} depend only on the geometry of the inhomogeneity and the Poisson's ratio of the surrounding material. If the material is poroelastic, then either the drained or undrained compliances could be used in Eq. (57), but the relation does not apply if flow occurs. An analogous time-dependent relation for a poroelastic solid, established only for a spherical inclusion [94], is discussed below.

6.1 Elastic surroundings

The relation (57) is independent of the properties of the inhomogeneity so long as they are uniform. For example, Rudnicki [95] has used a nonlinear relation between the stress and strain in the inhomogeneity to study the stability of faulting in a rock mass with a weakened zone. In particular, the properties of the inclusion may be taken as poroelastic and used to examine the response of reservoirs or aquifers to alterations in fluid mass or pore pressure [96]. If these alterations occur much more rapidly than any changes in far field

strain, then it is possible to take $\varepsilon^{\infty}_{mn}=0$. The stresses can then be eliminated from (57) using the ordinary elastic relation for the exterior and the poroelastic relation for the inclusion. The result is

$$\varepsilon_{mn}+\frac{1}{3}S_{mnkk}(k-g)e+gS_{mnkl}\varepsilon_{kl}=-\frac{\zeta}{K_{\infty}}pS_{mnkk} \qquad (58)$$

where $k=K/K_{\infty}-1$, $g=G/G_{\infty}-1$, and $e=\varepsilon_{kk}$ is the inclusion volume strain. Alternatively, the pore pressure could be eliminated in favor of the fluid mass or Eq. (58) could be expressed in terms of the stresses. If the inhomogeneity were completely unconstrained by the surroundings, then an alteration of pressure would cause a volume strain obtained from Eqs. (7) or (8) with $\sigma_{ij}=0$. If the inhomogeneity is spherical, then the strain resulting from pore pressure change is still purely volumetric but its magnitude depends on the mismatch of properties. In the limit of a vanishingly thin inhomogeneity, equivalent to a thin, layered geometry, the strain is uniaxial, ie, $\varepsilon_3=\varepsilon_2=0$, if the 1-axis is perpendicular to the plane of the inhomogeneity. More generally, for axisymmetric inhomogeneities, the ratio of the strain in the direction of the long axis to that in the direction of the short axis, $R=\varepsilon_3/\varepsilon_1$ can be obtained explicitly from (58). Figure 18 plots this ratio as a function of the aspect ratio $\xi\leqslant 1$ for $G/G_{\infty}=0.5$, 1.0, and 2.0. In Fig. 18, $\nu_{\infty}=0.2$, but the dependence on ν_{∞} is weak and R is independent of Poisson's ratio of the inhomogeneity. As shown by the figure, the strain caused by pressure changes is uniaxial in the limit $\xi\to 0$, but the approach to the limit depends on the ratio of shear moduli and is slower if the inhomogeneity is stiffer than the surroundings.

Because the stresses can be determined from the strains, this analysis also makes it possible to determine whether pressure changes cause the inhomogeneity stress state to move toward or away from some failure condition. Consider, for definiteness, fluid withdrawal (so that the pore pressure decreases) and a failure condition given by the Mohr-Coulomb condition with friction angle ϕ. Then fluid withdrawal will cause the stress state to move away from failure if the following inequality is satisfied

$$\zeta<\frac{2(1-\nu)}{(1-2\nu)}\left\{\frac{1+\dfrac{2\nu}{1-\nu}R}{1-R}\right\}\frac{\sin\phi}{1+\sin\phi} \qquad (59)$$

(This relation is derived assuming that the stress change in the direction of the short axis of the inhomogeneity is zero, a good approximation for small aspect ratios; Rudnicki [96] gives results without making this approximation). Figure 19 shows the maximum values of ζ satisfying (59) for values of ξ from zero to 0.2 and three values of G/G_{∞}: 0.5, 1.0, and 2.0. Results are plotted for $\nu=0.2$ and $\phi=25°$.

6.2 Poroelastic surroundings

As noted, the relation (57) does not apply if the material surrounding the inhomogeneity is poroelastic and flow occurs. Rice *et al* [94] have established the corresponding relation for a spherical inhomogeneity in a poroelastic solid. They accomplish this by solving the problem of a spherical cavity subjected to a traction derived from a purely deviatoric stress tensor at the cavity wall S_{ij} (Fig. 20). They show

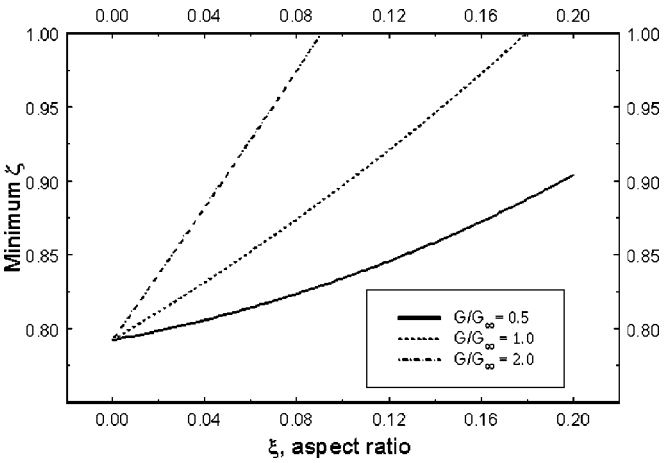

Fig. 19 Maximum values of ζ for which pressure decreases cause the stress state to move away from a Mohr-Coulomb failure with slope tan ϕ, with $\phi=25°$; plot is for $\nu=0.2$.

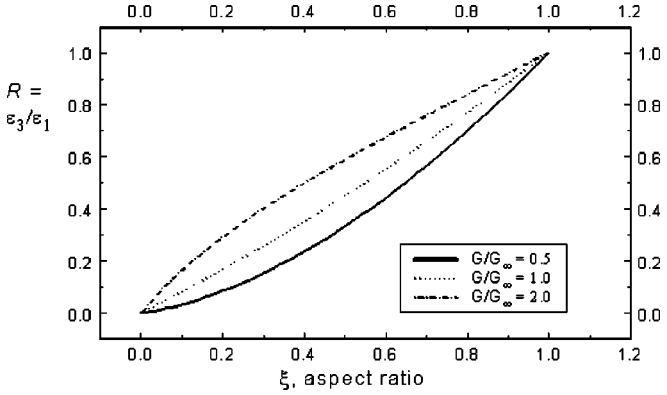

Fig. 18 Variation of strain state with aspect ratio and mismatch of shear modulus for pressure changes

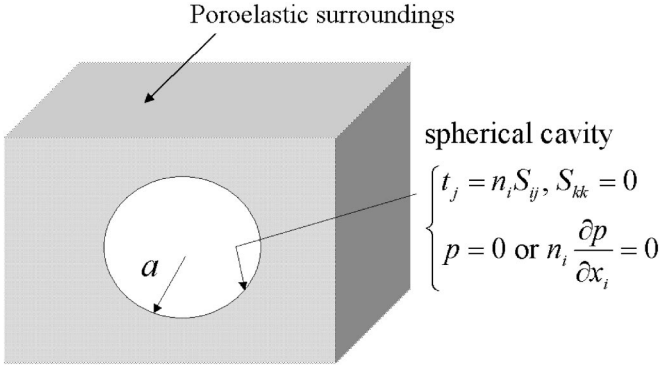

Fig. 20 Sketch of a spherical cavity in an infinite poroelastic solid. Cavity boundary is loaded by a traction derived from a uniform deviatoric stress, S_{ij}, $S_{kk}=0$. Cavity boundary is either permeable ($p=0$) or impermeable ($\partial p/\partial n=0$).

that the cavity wall deforms in a manner consistent with uniform strain of the interior:

$$Gu_i = H(t) S_{ij} x_j \tag{60}$$

where x_i is position and $H(t)$ is given by

$$H(t) = \frac{4-5\nu_u}{7-5\nu_u} + h(t)\left\{\frac{4-5\nu}{7-5\nu} - \frac{4-5\nu_u}{7-5\nu_u}\right\}. \tag{61}$$

The function $h(t)$ varies from zero at $t=0$, undrained response, to one as $t\to\infty$, drained response, but depends on whether the cavity boundary is permeable or impermeable. Rice *et al* [94] give and plot the result for the permeable boundary but give only the Laplace transform of the result for the impermeable boundary. The latter can, however, be inverted into an integral form convenient for numerical evaluation by using the procedure described in the Appendix of [94]. Figure 21 plots the results for both the permeable and impermeable boundaries for $\lambda=0.9$ where $\lambda=(1-\nu_u)\times(7-5\nu)/(1-\nu)(7-5\nu_u)$. (Rice *et al* [94] note that the practical range of λ is 7/9, for separately incompressible constituents, to 1.0).

Superposition and (60) are used to derive a relation for the *deviatoric* stress and strain components corresponding to (57):

$$G\{e_{ij} - e^{\infty}_{ij}\} = \int_{-\infty}^{t} H(t-t')\{\dot{S}^{\infty}_{ij}(t') - \dot{S}_{ij}(t')\}dt' \tag{62}$$

where the dot denotes the time derivative.

Rice *et al* [94] derive corresponding results for application of normal traction and pore pressure at the cavity wall from solutions given by [22]. The result for the normal traction leads to a relation for the volumetric components that is identical to Eq. (57) when specialized to a spherical inhomogeneity, isotropic surroundings, and volumetric components:

$$4G\{e(t) - e^{\infty}(t)\} = \sigma^{\infty}_{kk}(t) - \sigma_{kk}(t). \tag{63}$$

If the inhomogeneity boundary is impermeable, then the pore pressure change inside is given by the undrained response. If the boundary is permeable and it is assumed that there is no change in far field fluid mass content, then the fluid mass change in the inhomogeneity is related to the pore pressure there and the far field value by

$$\dot{m}(t) = -\frac{3\rho_0\kappa}{a^2}\left\{[p(t) - p^{\infty}(t)] + \int_{-\infty}^{t} \frac{a[\dot{p}(t') - \dot{p}^{\infty}(t')]}{[\pi c(t-t')]^{1/2}} dt'\right\}. \tag{64}$$

In order for p to be identified with the pore pressure of the inhomogeneity, the inhomogeneity must be much more permeable than the surroundings so that any non-uniformities in the pore pressure are equilibrated rapidly. This is likely to be a good approximation for the intended applications, aquifers, reservoirs, and fault zones.

Rice and Rudnicki [48] have used these results to study the effects of coupling between deformation and diffusion on earthquake precursory phenomena. They find that this coupling can transiently stabilize an inertial instability, corresponding to the occurrence of an earthquake, and give rise to period of self-driven, accelerating deformation. The duration of this period is of the order of 15–240 days for a spherical zone of radius 1 km but about an order of magnitude shorter for a flat elliptical zone. There are, however, a number of other effects that contribute to the processes prior to earthquakes and distinguishing them is difficult. In addition, the absence of reported precursors in well-instrumented areas suggests that such effects may be difficult to observe, if they do occur.

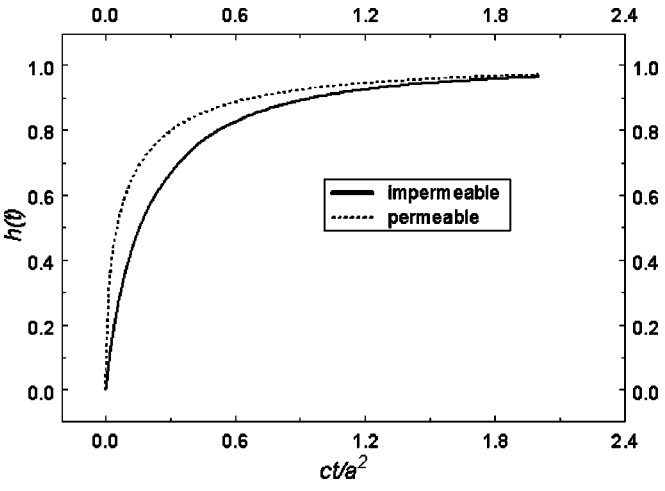

Fig. 21 Time dependence of the boundary shear strain for uniform shear stress applied to a spherical cavity

7 INELASTIC EFFECTS

The discussion has focused primarily on poroelastic effects; any inelasticity has been confined to the plane of the slip surface or fracture, although some results have included a nonlinear relation between the traction and relative displacement on the surface. Other inelastic effects can, however, be coupled with fluid diffusion. In particular, many rocks and granular materials dilate, or increase their pore volume, upon inelastic shearing. For granular materials, dilation results from rearrangement of grains into a less compact state; in rocks, it results from microcracking due to local tensile stresses and to uplift in sliding over asperities on frictional surfaces. If dilation occurs more rapidly than fluid can flow into the newly created void space, the pore pressure tends to decrease. Hence, the effective compressive stress for inelastic deformation (difference between the total compressive stress and pressure) increases. Because resistance to inelastic deformation for most geomaterials is inhibited by increases in effective stress, the response is stiffer and is said to be *dilatantly hardened* [25,97].

Rice [25] conducted an insightful analysis of the stability of dilatant hardening for a layer subjected to a combination of simple shear and compression. He showed that homogeneous dilatant hardening becomes unstable when the conditions for localization of deformation [98] are met in terms of the underlying drained response. The response is unstable in the sense that infinitesimal spatial perturbations grow expo-

nentially in time once conditions for localization are met in terms of the drained response. Rudnicki [99] has shown that a similar result applies for arbitrary deformation states: infinitesimal spatial nonuniformities begin to grown exponentially when the condition for localization is met in terms of the drained response. The growth rate does not necessarily become unbounded, as it does for the layer, when the localization condition is met in terms of the undrained response. This difference is due to an absence of symmetry in the constitutive tensor that is typical of geological materials.

Because the analysis of [25] was limited to small perturbations from homogeneous deformation, Rudnicki [100] examined the effects of dilatant hardening on the concentration of deformation in an inelastically deforming rock mass containing an initially weakened layer of thickness h and loaded in the far field by a constant rate of shear $\dot{\gamma}_\infty$. For tectonic applications and most laboratory experiments, the ratio $\dot{\gamma}_\infty h^2/c$, where c is a diffusivity, is small. In this case, a nonlinear asymptotic analysis predicts that occurrence of instability is delayed by dilatant hardening for a time given by

$$t_{delay} \propto (\alpha h^2/c)^{2/3} (\Gamma/\dot{\gamma}_\infty)^{1/3} \Delta^{-1/6} \tag{65}$$

where Γ is the half-width of the peak of the stress strain curve, Δ is the ratio of the difference in the peak stresses of the rock mass and the weakened layer to Γ times the elastic shear modulus, and α is a nondimensional measure of the strength of dilatant hardening. For a range of numerical values, the delay times are very short: less than a few hours for tectonic strain rates and less than a few tens of seconds for typical laboratory strain rates.

Rudnicki's analysis [100] was motivated, in part, by laboratory observations by [101] on the pore fluid stabilization of failure in axisymmetric compression samples of Westerly granite. Martin [101] observed that for pore pressures in a reservoir connected to the sample that exceeded a critical value, failure took place slowly, on the order of several hundred seconds, rather than abruptly. Because the delay times (65) predicted by [100] were so much shorter than the several hundred seconds observed by [101], Rudnicki [100] concluded that the observed stabilization could not be attributed to dilatant hardening effects on shear localization. As an alternative, Rudnicki and Chen [102] suggested that Martin's [101] samples had already localized and that the stabilization he observed was associated with dilatant uplift accompanying frictional slip. In the analysis of [102], dilatant hardening prevents the occurrence of instability if the reservoir (initial) pore pressure is sufficiently high: if reductions of pore pressure caused by dilatant hardening exceed the initial pore pressure, rapid reduction of the fluid bulk modulus eliminates the stabilizing effect. Results from this analysis [102] agree well with the critical pressure observed by [101] and are consistent with the trends of decreasing critical reservoir pressure with increasing effective confining stress and decreasing applied strain rate. Furthermore, Vardoulakis (personal communication, 1994) has reported observations consistent with cavitation of pore fluid in the interior of dilating specimens.

Rudnicki and Chen's analysis [102] assumed that shear stress on the fault or frictional surface evolved only with slip displacement and that dilatancy, or opening of the surface, was related to this slip. Segall and Rice [103] analyzed a fluid-infiltrated fault using a more elaborate friction model in which the shear stress depends on the rate of slip and an evolving state variable that reflects the past history of sliding [104–106]. They also include dilatancy and pore compaction in a manner consistent with experiments of [107]. The linearized stability analysis they perform shows that the critical stiffness, below which instability occurs, deceases with the transition from drained to undrained conditions. For undrained conditions and sufficient magnitude of dilatancy, slip is always stable for small perturbations. The result implies a limit to magnitude of the pore pressure for which undrained conditons are stable. Simulations performed by [103] indicate a variety of interesting behaviors, including the occurrence of large aftershock-like events succeeding a major slip event. Chambon and Rudnicki [108] have recently extended the analysis of [103] to include normal stress variations typical of axisymmetric compression tests or normal faults near a free surface. Among the effects they find is that the critical stiffness for linearized instability does not vary monotonically between drained and undrained conditions when normal stress variations are included.

Pietruszczak [109] has recently used a layer analysis similar to that of [100] to consider plane strain deformation in the limits of locally drained and locally undrained response. He finds that the results satisfactorily model experimental observations of Han and Vardoulakis [110] on dense sand. Rudnicki and Smith [111] and Garagash and Rudnicki [112] have extended the formulation of [102] to include increases in pore pressure due to frictional heating as a model for earthquake instability at midcrustal depths.

Vardoulakis [113] has extended the linear perturbation analysis of [25] to consider compacting materials. Since compaction tends to increase the pore pressure in undrained samples, the effective compressive stress decreases and the response is softened. Hence, conditions for shear localization may be met earlier for undrained response than for drained response. Vardoulakis [113] showed that when the condition for localization is met in terms of the undrained response, the growth rate of infinitesimal spatial nonuniformities changes from large negative to large positive values. This result applies when the resistance to inelastic deformation increases with an increase in effective compressive stress. But, as noted by [114], for materials modelled by a *cap* [115] on the yield surface, the resistance to inelastic deformation decreases with an increase in effective compressive stress. Rudnicki [99] points out that for a material of this type that compacts inelastically, the results for diffusive instability are identical to those for the dilatant hardening material analyzed by [25], at least from the point of view of the linear perturbation analysis.

The experiments of [107,116] on simulated fault gouge and of [117,118] on sands indicate both compaction and dilation. Consequently, the development of localized deformation can be affected by the relative rates and magnitudes of compaction and dilation and the rate at which fluid mass is exchanged between local non-uniformities and adjacent ma-

terial. Rudnicki [119] and Rudnicki *et al* [120] have suggested this as an explanation for evanescent shear bands observed using stereophotogrammetry by [117,118] in biaxial compression of sand. The preliminary analyses of [119,120] suggest that relatively small variations in the porosity response can strongly alter the undrained behavior and, possibly, the development of shear localization.

8 CONCLUDING DISCUSSION

This paper has discussed a variety of effects of coupling between deformation and fluid diffusion on slip and fracture in the Earth's crust and on the failure of geomaterials. Both laboratory and *in situ* observations and estimates based on plausible values of material parameters suggest that these effects can be significant. Uncertainties arise, however, because material and transport properties are often not well constrained and because adequate coverage is difficult to achieve in field observations. Although the formulation and solution methods of poroelasticity are well-established, applications are often hindered by uncertainty about the significance of inelastic effects and the incompleteness of their characterization.

ACKNOWLEDGMENT

This article is based on the text of a keynote lecture at the *Biot Conference on Poromechanics*, Louvain-La-Neuve, Belgium, September 14–16, 1998. I am grateful to the organizers, J-F Thimus, Y Abousleiman, AH-D Cheng, O Coussy, and E Detournay for the invitation to participate. I am also grateful for financial support of my research related to the topic of this paper from the Geosciences Program of the Basic Energy Sciences of the US Department of Energy, the Earth Sciences Division of the US National Science Foundation, and the Earthquake Hazards Reduction Program of the US Geological Survey.

REFERENCES

[1] Kerr RA (1993), Looking-deeply-into the Earth's crust in Europe, *Science* **261**, 295–297.
[2] Kerr RA (1994), German super-deep hole hits bottom, *Science* **266**, 545.
[3] Kennedy BM, Kharaka YK, Evans WC, Ellwood A, DePaolo DJ, Thordsen J, Ambats G, and Mariner RH (1997), Mantle fluids in the San Andreas Fault system, California, *Science* **278**, 1278–1281.
[4] Rudnicki JW (2000), Geomechanics, *Int. J. Solids Struct.* **37**, 349–358.
[5] Roeloffs EA (1988), Hydrologic precursors to earthquakes: A review, *Pure Appl. Geophys.* **126**, 177–209.
[6] Roeloffs EA (1996), Poroelastic methods in the study of earthquake-related phenomena, in *Advances in Geophysics*, Dmowska R (ed), Academic Press, San Diego CA **37**, 135–195.
[7] Hickman SR, Sibson R, and Bruhn R (1995), Introduction to special section: Mechanical involvement of fluids in faulting, *J. Geophys. Res.* **100**, 12,831–12,840.
[8] Ingebritsen SE and Rojstaczer SA (1993), Controls on geyser periodicity, *Science* **262**, 889–892.
[9] Johnson CE (1979), I. CEDAR—An approach to the computer automation of short-period local seismic networks: II Seismotectonics of the Imperial Valley of sourthern California, PhD Thesis, California Inst of Tech, Pasadena CA.
[10] Elsworth D and Voight B (1992), Theory of dike intrusion in a saturated porous solid, *J. Geophys. Res.* **97**, 9105–9117.
[11] Elsworth D, Voight B, Ouyang Z, and Piggott AR (1996), Poroelastic response resulting from magma intrusion, in *Mechanics of Poroelastic Media*, APS Selvadurai (ed), Kluwer Academic Publ, Netherlands, 215–233.
[12] Blakeslee S (1992), Quake theory attacks prevailing wisdom on how faults slide, New York Times, April 14, pp. B5, B8.
[13] Kerr RA (1992), Weak faults: Breaking out all over, *Science* **255**, 1210–1212.
[14] Zhao D, Kanamori H, Negishi H, and Wiens D (1996), Tomography of the source area of the 1995 Kobe earthquake: Evidence for fluids at the hypocenter?, *Science* **274**, 1891–1894.
[15] Peltzer G, Rosen P, Rogez F, and Hudnut K (1996), Postseismic rebound in fault step-overs caused by pore fluid flow, *Science* **273**, 1202–1204.
[16] King C-Y, Koizumi N, and Kitagawa Y (1995), Hydrochemical anomalies and the 1995 Kobe earthquake, *Science* **269**, 38–39.
[17] Wawersik WR, Rudnicki JW, Dove P, Harris J, Logan JM, Pyrak-Nolte L, Orr FM Jr, Ortoleva PJ, Richter F, Warpinski NR, Wilson JL, and Wong T-f (2000), Terrestrial sequestration of CO_2: An assessment of research needs, in *Advances in Geophysics*, Dmowska R (ed), **43**, 97–177.
[18] Biot MA (1941), General theory of three dimensional consolidation, *J. Appl. Phys.* **12**, 155–164.
[19] Detournay E and AH-D Cheng (1991), Fundamentals of poroelasticity, in *Comprehensive Rock Engineering: Principles, Practice & Projects*, Hudson JA (ed), Pergamon New York, Vol 2, Ch 5, 113–171.
[20] Coussy O (1995), *Mechanics of Porous Continua*, New York: Wiley.
[21] Wang HF (2000), *Theory of Linear Poroelasticity with Applications to Geomechanics and Hydrology*, Princeton Univ Press, 276 pp.
[22] Rice JR and Cleary MP (1976), Some basic stress diffusion solutions for fluid-saturated elastic porous media with compressible constituents, *Rev. Geophys. Space Phys.* **14**, 227–241.
[23] Coussy O, Dormieux L, and Detournay E (1998), From mixture theory to Biot's approach for porous media, *Int. J. Solids Struct.* **35**, 4619–4635.
[24] Biot MA (1973), Nonlinear and semilinear rheology of porous solids, *J. Geophys. Res.* **78**, 4924–4937.
[25] Rice JR (1975), On the stability of dilatant hardening for saturated rock masses, *J. Geophys. Res.* **80**, 1531–1536.
[26] Nur A and Byerlee JD (1971), An exact effective stress law for elastic deformation of rock with fluids, *J. Geophys. Res.* **76**, 6414–6419.
[27] Cornet FH and Fairhurst C (1974), Influence of pore pressure on the deformation behavior of saturated rocks, in *Proc of 3rd Congress of the Int Soc for Rock Mechanics*, Vol 1, Part B, 638–644, National Academy of Sciences, Washington DC.
[28] Biot MA and Willis DG (1957), The elastic coefficients of the theory of consolidation, *ASME J. Appl. Mech.* **24**, 594–601.
[29] Geertsma J (1966), Problems of rock mechanics in petroleum engineering, in *Proc of 1st Congress Int Soc of Rock Mechanics*, Lisbon: Labatorio Nacional de Engenharia Civil, National Laboratory of Civil Engineering, Lisbon, 585–594.
[30] Geertsma J (1973), Land subsidence above compacting oil and gas reservoirs, *J. Pet. Technol.* **25**, 734–744.
[31] Segall P (1989), Earthquakes triggered by fluid extraction, *Geology* **17**, 942–946.
[32] Segall P (1992), Induced stresses due to fluid extraction from axisymmetric reservoirs, *Pure Appl. Geophys.* **139**, 535–560.
[33] Segall P, Grasso JR, and Mossop A (1994), Poroelastic stressing and induced seismicity near the Lacq gas field, southwestern France, *J. Geophys. Res.* **99**, 15,423–15,438.
[34] Rice JR (1980), Pore fluid processes in the mechanics of earthquake rupture, in *Solid Earth Geophysics and Geotechnology*, Nemat-Nasser S (ed), ASME Applied Mechanics Vol. **37**, 81–89.
[35] Rudnicki JW (1986), Fluid mass sources and point forces in linear elastic diffusive solids, *Mech. Mater.* **5**, 383–393.
[36] Rudnicki JW (1996), Moving and stationary dislocations in poroelastic solids and applications to aseismic slip in the Earth's crust, in *Mechanics of Poroelastic Media*, Selvadurai APS (ed), Kluwer Academic Publ, Netherlands, 3–22.
[37] Cleary MP (1977), Fundamental solutions for a fluid-saturated porous solid, *Int. J. Solids Struct.* **13**, 785–808.
[38] Segall P (1985), Stress and subsidence resulting from subsurface fluid withdrawal in the epicentral region of the 1983 Coalinga earthquake, *J. Geophys. Res.* **90**, 6801–6816.
[39] Roeloffs E (1982), Elasticity of saturated porous rocks: Laboratory measurements and a crack problem, PhD thesis, Univ of Wisconsin, Madison, WI.
[40] Fatt I (1958), The compressibility of sandstones at low to moderate pressures, *Bull. Am Assoc. Pet. Geol.* **42**, 1924–1957.
[41] Fatt I (1959), The Biot-Willis coefficients for a sandstone, *ASME J. Appl. Mech.* **26**, 296–297.

[42] Mann KL and Fatt I (1960), Effects of pore fluids on the elastic properties of sandstone, *Geophysics* **25**, 433–444.
[43] Roeloffs EA and Rudnicki JW (1984/85), Coupled deformation-diffusion effects on water-level changes due to propagating creep waves, *Pure Appl. Geophys.* **122**, 560–582.
[44] Roeloffs EA (1988), Fault stability changes induced beneath a reservoir with cyclic variations in water level, *J. Geophys. Res.* **93**, 2107–2124.
[45] Mesri G, Adachi K, and Ullrich CR (1976), Pore pressure response in rock to undrained change in all-round stress, *Geotechnique* **26**, 317–330.
[46] Green DH and Wang HF (1986), Fluid pressure response to undrained compression in saturated sedimentary rock, *Geophysics* **51**, 948–956.
[47] Brace WF (1965), Some new measurements of the linear compressibility of rocks, *J. Geophys. Res.* **70**, 391–398.
[48] Rice JR and Rudnicki JW (1979), Earthquake precursory effects due to pore fluid stabilization of a weakening fault zone, *J. Geophys. Res.* **84**, 2177–2193.
[49] O'Connell RJ and Budiansky B (1977), Viscoelastic properties of fluid saturated cracked solids, *J. Geophys. Res.* **82**, 5719–5735.
[50] Beavan J, Evans K, Mousa S, and Simpson DW (1991), Estimating aquifer parameters from analysis of force fluctuations in well level: an example from the Nubian Formations near Aswan, Egypt 2. Poroelastic properties, *J. Geophys. Res.* **96**, 12,139–12,160.
[51] O'Connell RJ and Budiansky B (1974), Seismic velocities in dry and saturated cracked solids, *J. Geophys. Res.* **79**, 5412–5426.
[52] Anderson DL and Whitcomb JH (1975), Time dependent seismology, *J. Geophys. Res.* **80**, 1497–1503.
[53] Rice JR and Simons DA (1976), The stabilization of spreading shear faults by coupled deformation-diffusion effects in fluid-infiltrated porous materials, *J. Geophys. Res.* **81**, 5322–5344.
[54] Kovach RL, Nur A, Wesson RL, and Robinson R (1975), Water level fluctuations and earthquakes on the San Andreas fault zone, *Geology* **3**, 437–440.
[55] Fletcher JB and Sykes LR (1977), Earthquakes related to hydraulic mining and natural seismic activity in western New York state, *J. Geophys. Res.* **82**, 3767–3780.
[56] Li VC (1984/85), Estimation of in-situ hydraulic diffusivity of rock masses, *Pure Appl. Geophys.* **122**, 546–559.
[57] Talwani P and Acree S (1984/85), Pore pressure diffusion and the mechanism of reservoir induced seismicity, *Pure Appl. Geophys.* **122**, 947–965.
[58] Lippincott DK, Bredehoeft JD, and Moyle WR Jr., (1985), Recent movement on the Garlock Faut suggested by water level fluctuations in a well in Fremont Valley, California, *J. Geophys. Res.* **90**, 1911–1924.
[59] Rudnicki JW and Hsu T-C (1988), Pore pressure changes induced by slip on permeable and impermeable faults, *J. Geophys. Res.* **93**, 3275–3285.
[60] Rudnicki JW, Yin J, and Roeloffs EA (1993), Analysis of water level changes induced by fault creep at Parkfield, California, *J. Geophys. Res.* **98**, 8143–8152.
[61] Roeloffs EA, Burford SS, Riley FS, and Records AW (1989), Hydrologic effects on water level changes associated with episodic fault creep near Parkfield, California, *J. Geophys. Res.* **94**, 12,387–12,402.
[62] Cleary MP (1978), Moving singularities in elasto-diffusive solids with applications to hydraulic fracture, *Int. J. Solids Struct.* **14**, 81–97.
[63] Detournay E and Cheng AH-D (1987), Poroelastic solution of a plane strain point displacement discontinuity, *ASME J. Appl. Mech.* **109**, 783–787.
[64] Vandamme L, Detournay E, and Cheng AH-D (1989), A two-dimensional poroelastic displacement discontinuity method for hydraulic fracture simulation, *Int. J. Numer. Analyt. Meth. Geomech.* **13**, 215–224.
[65] Nur A and Booker JR (1972), Aftershocks caused by fluid flow, *Science* **175**, 885–887.
[66] Booker JR (1974), Time-dependent strain following faulting of a porous medium, *J. Geophys. Res.* **79**, 2037–2044.
[67] Wu FT, Blatter L, and Roberson H (1975), Clay gouges in the San Andreas fault system and their possible implications, *Pure Appl. Geophys.* **113**, 87–95.
[68] Wang C-Y and Lin W (1978), Constitution of the San Andreas fault zone at depth, *Geophys. Res. Lett.* **5**, 741–744.
[69] Rudnicki JW (1986), Slip on an impermeable fault in a fluid-saturated rock mass, in *Earthquake Source Mechanics*, Das S, Boatwright J, and Scholz CH (eds), Geophys. Monogr. Ser. American Geophysical Union, Washington DC, Vol **37**, 81–89.
[70] Abramowitz M and Stegun I (eds) (1967), *Handbook of Mathematical Functions*, National Bureau of Standards, Applied Mathematics Series 55.
[71] Rudnicki JW (1987), Plane strain dislocations in linear elastic diffusive solids, *ASME J. Appl. Mech.* **109**, 545–552.
[72] Rudnicki JW and Roeloffs EA (1990), Plane-strain shear dislocations moving steadily in linear elastic diffusive solids, *ASME J. Appl. Mech.* **112**, 32–39.
[73] Simons DA (1979), The analysis of propagating slip zones in porous elastic media, in *Fracture Mechanics, Proc of the Symp in Applied Mathematics of AMS and SIAM*, Burridge R (ed), 153–169.
[74] Johnson AG, Kovach RL, and Nur A (1973), Pore pressure changes during creep events on the San Andreas fault, *J. Geophys. Res.* **78**, 851–857.
[75] Wesson RL (1981), Interpretation of changes in water level accompanying fault creep and implications for earthquake prediction, *J. Geophys. Res.* **86**, 9259–9267.
[76] Rudnicki JW and Wu M (1993), Pore pressure changes induced by slip in a poroelastic half-space, in Final Technical Report to US Geological Survey for Award No 1434-92-G-2164.
[77] Rice JR (1980), The mechanics of earthquake rupture, in *Physics of the Earth's Interior (Proc of Int Sch of Physics*, "Enrico Fermi," Course 78, 1979), Dziewonski AM and Boschi E (eds), 555–649.
[78] Rudnicki JW (1979), The stabilization of slip on a narrow weakening fault zone by coupled-deformation pore fluid diffusion, *Bull. Seismol. Soc. Am.* **69**, 1011–1026.
[79] Koutsibelas DA (1988), Stabilization of slip in a fluid-infiltrated rock mass, PhD Thesis, Northwestern Univ, Evanston, IL.
[80] Tse ST and Rice JR (1986), Crustal earthquake instability in relation to the depth variation of frictional slip properties, *J. Geophys. Res.* **91**, 9452–9472.
[81] Rice JR (1968), Mathematical analysis in the mechanics of fracture, in *Fracture: An Advanced Treatise* 2, Liebowitz H (ed), Academic Press, New York, 191–311.
[82] Rudnicki JW and Koutsibelas DA (1991), Steady propagation of plane strain shear cracks on an impermeable plane in an elastic diffusive solid, *Int. J. Solids Struct.* **27**, 205–225.
[83] Paterson MS (1978), *Experimental Rock Deformation The Brittle Field*, Springer-Verlag, New York.
[84] Rice JR (1977), Pore pressure effects in inelastic constitutive formations for fissured rock masses, in *Advances in Civil Engineering through Engineering Mechanics*, ASCE, 360–363.
[85] Simons DA (1977), Boundary-layer analysis of propagating Mode II cracks in porous elastic solids, *J. Mech. Phys. Solids* **25**, 99–116.
[86] Rudnicki JW (1991), Boundary layer analysis of plane strain shear cracks propagating steadily on an impermeable plane in an elastic diffusive solid, *J. Mech. Phys. Solids* **39**, 201–221.
[87] Craster RV and Atkinson C (1992), Shear cracks in thermoelastic and poroelastic media, *J. Mech. Phys. Solids* **40**, 887–924.
[88] Craster RV and Atkinson C (1994), Crack problems in a poroelastic material: an asymptotic approach, *Philos. Trans. R. Soc. London* **A346**, 387–428.
[89] Ruina A (1978), Influence of coupled deformation-diffusion effects on retardation of hydraulic fracture, in *Proc of 19th US Symp on Rock Mechanics*, Kim YS (ed), University of Nevada-Reno, 274–282.
[90] Atkinson C and Craster RV (1991), Plane strain fracture in poroelastic media, *Proc. Roy. Soc.* **A434**, 605–633.
[91] Craster RV and Atkinson C (1992), Interfacial fracture in diffusive elastic media, *Int. J. Solids Struct.* **29**, 1463–1498.
[92] Craster RV and Atkinson C (1996), Theoretical aspects of fracture in porous elastic media, in *Mechanics of Poroelastic Media*, Selvadurai APS (ed), Kluwer Academic Publ, Netherlands, 23–45.
[93] Eshelby JD (1957), The determination of the elastic field of an ellipsoidal inclusion and related problems, *Proc. Roy. Soc. London* **A241**, 376–396.
[94] Rice JR, Rudnicki JW, and Simons DA (1978), Deformation of spherical cavities and inclusions in fluid-infiltrated elastic materials, *Int. J. Solids Struct.* **14**, 289–303.
[95] Rudnicki JW (1977), The inception of faulting in a rock mass with a weakened zone, *J. Geophys. Res.* **82**, 844–854.
[96] Rudnicki JW (1999), Alteration of regional stress by reservoirs and other inhomogeneities, in *Proc 9th Intl Congress on Rock Mechanics*, Vouille G and Berest P (eds), Paris, Vol. 3, Balkema, Rotterdam.
[97] Rudnicki JW (1985), Effect of pore fluid diffusion on deformation and failure of rock, in *Mechanics of Geomaterials*, Bažant ZP (ed), John Wiley & Sons, New York, 315–347.
[98] Rudnicki JW and Rice JR (1975), Conditions for the localization of deformation in pressure-sensitive dilatant materials, *J. Mech. Phys. Solids* **23**, 371–394.

[99] Rudnicki JW (2000), Diffusive instabilities in dilating and compacting geomaterials, in *Multiscale Deformation and Fracture in Materials and Structures*, Chuang T-J and Rudnicki JW (eds), Kluwer Academic Publ, 159–182.
[100] Rudnicki JW (1984), Effects of dilatant hardening on the development of concentrated shear deformation in fissured rock masses, *J. Geophys. Res.* **89**, 9259–9270.
[101] Martin RJ III (1980), Pore fluid stabilization of failure in Westerly granite, *Geophys. Res. Lett.* **7**, 404–406.
[102] Rudnicki JW and Chen C-H (1988), Stabilization of rapid frictional slip on a weakening fault by dilatant hardening, *J. Geophys. Res.* **93**, 4745–4757.
[103] Segall P and Rice JR (1995), Dilatancy, compaction, and slip instability of a fluid-infiltrated fault, *J. Geophys. Res.* **100**, 22,155–22,171.
[104] Dieterich JH (1978), Time-dependent friction and the mechanics of stick-slip, *Pure Appl. Geophys.* **143**, 425–456.
[105] Dieterich JH (1979), Modeling of rock friction, 1, Experimental results and constitutive equations, *J. Geophys. Res.* **84**, 2161–2168.
[106] Ruina A (1983), Slip instability and state variable friction laws, *J. Geophys. Res.* **88**, 10,359–10,370.
[107] Marone C, Raleigh CB, and Scholz CH (1990), Frictional behavior and constitutive modeling of simulated fault gouge, *J. Geophys. Res.* **95**, 7007–7025.
[108] Chambon G and Rudnicki JW (2001), Effects of normal stress variations on frictional stability of a fluid-infiltrated fault, *J. Geophys. Res.* **106**, 11,353–11,372.
[109] Pietruszczak S (1995), Undrained response of granular soil involving localized deformation, *J. Eng. Mech.* **121**, 1292–1297.
[110] Han C and Vardoulakis I (1991), Plane strain compression experiments on water-saturated fine grained sand, *Geotechnique* **41**, 49–78.
[111] Rudnicki JW and Smith K (1997), Shear heating of a fluid-saturated slip-weakening fault zone, *Trans. Geophys. Union* **78**, F477.
[112] Garagash D and Rudnicki JW (1999), Shear heating and slip instability of a fluid-saturated dilatant fault, *Trans. Am. Geophys. Union* **80**, F682.
[113] Vardoulakis I (1985), Stability and bifurcation of undrained, plane rectilinear deformations on water-saturated granular soils, *Int. J. Numer. Analyt. Meth. Geomech.* **9**, 399–414.
[114] Olsson WA (1999), Theoretical and experimental investigation of compaction bands, *J. Geophys. Res.* **104**, 7219–7228.
[115] Dimaggio FL and Sandler IS (1971), Material model for granular soils, *J. Eng. Mech.* **47**, 149–165.
[116] Marone C and Kilgore B (1993), Scaling of the critical slip distance for seismic faulting with shear strain in fault zones, *Nature (London)* **362**, 618–621.
[117] Finno RJ, Harris WW, Mooney MA, and Viggiani G (1996), Shear bands in plane strain compression of loose sand, *Geotechnique* **47**, 149–165.
[118] Finno RJ, Harris WW, Mooney MA, and Viggiani G (1996), Strain localization and undrained steady state of sand, *J. Geotech. Eng.* **122**, 462–473.
[119] Rudnicki JW (1996), Development of localization in undrained deformation, in *Proc of 11th Conf. Eng. Mech. Div.,* Lin YK and Su TC (ed), ASCE, New York, 939–942.
[120] Rudnicki JW, Finno RJ, Alarcon MA, Viggiani G, and Mooney MA (1996), Coupled deformation-pore fluid diffusion effects on the development of localized deformation in fault gouge, in *Prediction and Performance in Rock Mechanics and Rock Engineering,* EUROCK'96, Turin, Italy, Barla G (ed), Rotterdam: Balkema, 1261–1268.

After earning his ScB, ScM, and PhD degrees in engineering at Brown University, ***John W Rudnicki*** *was a postdoctoral research fellow in geophysics at Caltech for 18 months, and then Assistant Professor in the Department of Theoretical and Applied Mechanics at the University of Illinois in Urbana-Champaign for three years. In 1981, he moved to Northwestern University where he is now Professor in the Civil and Mechanical Engineering Departments. He has been interested in the inelastic behavior, failure and fracture of geological materials, and applications to the mechanics of earthquakes, the storage and recovery of energy, and disposal of toxic wastes. He has a held a variety of editorial and committee assignments, including terms as associate editor of the* Journal of Applied Mechanics *and the* Journal of Geophysical Research, *chairman of the Geomechanics committee of the ASME Applied Mechanics Division and as a member of the US National Committee on Rock Mechanics.*